Anomalous resistivity and heating in current-driven plasma thrusters*

E. Y. Choueiri†
Electric Propulsion and Plasma Dynamics Laboratory, Princeton University, Princeton, New Jersey 08544

(Received 20 November 1998; accepted 28 January 1999)

A theory is presented of anomalous resistivity and particle heating in current-driven plasma accelerators such as the magnetoplasmadynamic thruster (MPDT). An electromagnetic dielectric tensor is used for a current-carrying, collisional and finite-beta plasma and it is found that an instability akin to the generalized lower hybrid drift instability (GLHDI) exists for electromagnetic modes (i.e., with finite polarization). Weak turbulence theory is then used to develop a second-order description of the heating rates of particles by the waves and the electron-wave momentum exchange rate that controls the anomalous resistivity effect. It is found that the electron Hall parameter strongly scales the level of anomalous dissipation for the case of the MPDT plasma. This scaling has recently been confirmed experimentally [Phys. Plasmas **5**, 3581 (1997)]. Polynomial expressions of the relevant transport coefficients cast solely in terms of macroscopic parameters are also obtained for including microturbulence effects in numerical plasma fluid models used for thruster flow simulation. © *1999 American Institute of Physics.* [S1070-664X(99)95705-1]

I. INTRODUCTION

Current-driven microinstabilities of a magnetized, current-carrying, and collisional plasma and their impact on transport have not been well studied in the regime where the plasma beta is finite. Aside from its fundamental value, this problem is relevant to the understanding of dissipation in some current-driven plasma devices.

The magnetoplasmadynamic thruster (MPDT) is an electromagnetic plasma accelerator intended for spacecraft propulsion. It is essentially a coaxial device in which a high-current discharge ionizes a gas and accelerates it to high exhaust velocities through the action of the Lorentz force produced by the interaction between the current flowing through the plasma and a self-induced or applied magnetic field. The MPDT can attain exhaust velocities in the range of 10–80 km/s with thrust efficiencies exceeding 40%.[1] References 1–4 give a review of research on MPDT starting from its inception.[5] The MPDT plasma has an electron temperature between 1 and 3 eV, an ion temperature between 1 and 10 eV and an electron density between 10^{13} and $10^{16}\,\mathrm{cm}^{-3}$ depending on the power level. Current densities and induced magnetic fields can reach as high as $10^3\,\mathrm{A/cm}^2$ and 1 kG in the megawatt-class devices. The electron Hall parameter and the plasma beta both range between 1 and 10. A more detailed description of the MPDT plasma can be found in Ref. 6.

The acceleration process in Lorentz force electromagnetic plasma accelerators such as the MPDT is current-driven with the thrust increasing with the square of the total current.[4] It is also known that the current can drive microinstabilities in the thruster plasma which may, through induced microturbulence, substantially increase dissipation and adversely impact the efficiency. The presence of current-driven microinstabilities in such accelerator plasmas have been established experimentally in the plasma of the MPDT at both low and high power levels.[7,8]

We have previously presented in conference papers[8,9] a theoretical treatment of microinstabilities and their effects on transport. Although the transport coefficients, especially the anomalous resistivity, derived in that work proved helpful in rendering numerical fluid simulations of MPDT flows more realistic,[10,11] a direct experimental proof of the existence of anomalous resistivity in such thrusters was not obtained until the recent measurements of Black *et al.*[12] (1997). In that work, the measured anomalous resistivity was found to scale in accordance with the previous theoretical predictions in Ref. 9. This experimental confirmation prompted the publication of the theoretical work in the present paper.

Previous attempts to model linear instabilities in the MPDT (Refs. 13, 14) and their effects on transport[14] have been limited to electrostatic modes, i.e., zero plasma beta, a condition difficult to justify for the plasma of such devices.

Finite-beta effects have been thought to be globally stabilizing,[15–17,14] especially for drift velocities exceeding the Alfvén velocity. We show that, for such plasmas, a finite beta can actually result in the excitation of finite-growth modes with mixed polarization. These effects not only alter the character of the linear modes, but affect the magnitude of the resulting anomalous transport.

We start in Sec. II with the linear stability description of a magnetoactive, current-carrying, collisional and finite-beta plasma and show that finite-beta effects which result in unstable modes with finite polarization are important for the MPDT plasma. For the MPDT plasma the dominant modes have charactersitic frequencies near the lower hybrid frequency ω_{lh} and the instability is the collisional analog of the collisionless case termed ''generalized lower hybrid drift instability'' (GLHDI) by Hsia *et al.*[18]

In Sec. III we outline the basic formalism we adopt for our formulation of anomalous transport. In Sec. IV we use

*)Paper F3I2.3 Bull. Am. Phys. Soc. **43**, 1704 (1998).
†Invited speaker.

the statistical description of the previous section to derive general *finite-beta* expressions for the anomalous ion and electron heating rates as well as for the electron-wave momentum exchange rate that controls the anomalous resistivity effect. These expressions are cast as integrals in wave vector space of quantities that depend on the various elements of the linear dispersion tensor derived in Sec. II, on the roots of the linear dispersion relation and on the saturation energy density of the fluctuating (turbulent) fields denoted by $\mathscr{E}_t$.

We then turn our attention in Sec. V to the difficult question of the saturation mechanism that dictates the magnitude and dependencies of $\mathscr{E}_t$. We consider four models for $\mathscr{E}_t$ based on four possible saturation mechanisms.

In Sec. VI we show various calculations of the anomalous heating and momentum exchange rates for plasma parameters of interest and compare their magnitudes to classical values.

We finally conclude in Sec. VII by using these calculations to arrive at polynomial expressions of the relevant transport coefficients cast solely in terms of macroscopic parameters for inclusion in numerical plasma fluid models used for thruster flow simulation.

II. THE DISPERSION TENSOR OF A CURRENT-CARRYING AND COLLISIONAL PLASMA

We seek a general kinetic description of the response of a collisional and magnetoactive plasma carrying a cross-field current to small perturbations without making the electrostatic assumption.

A. Stating the problem

Our entire problem can be formulated, as shown below, to be contained in the following matrix equation:

$$\begin{pmatrix} R_{xx} & R_{xy} & R_{xz} \\ R_{yx} & R_{yy} & R_{yz} \\ R_{zx} & R_{zy} & R_{zz} \end{pmatrix} \begin{pmatrix} E_x^{(1)} \\ E_y^{(1)} \\ E_z^{(1)} \end{pmatrix} = 0, \tag{1}$$

where the superscript 1 denotes the first-order harmonic part of the linearly perturbed quantities (in this case, the components of the electric field vector **E**). In the above equation, R_{ij} represent the elements of the *dispersion tensor* $\mathbf{R}(\omega,\mathbf{k})$ and are generally complex functions of the frequency ω and wave vector **k** of the oscillations as well as of all the plasma parameters of the problem. As usual the dispersion relation is obtained from

$$\det|R_{ij}(\omega,\mathbf{k})| = 0. \tag{2}$$

In this section we outline the derivation of explicit expressions for the elements R_{ij} needed for our study.

B. Defining the problem in terms of the conductivity, dielectric, and dispersion tensors

The conductivity tensor $\boldsymbol{\sigma}$ and the dielectric tensor **K** are defined by

$$\mathbf{j}^{(1)} = \boldsymbol{\sigma}\mathbf{E}^{(1)}, \tag{3}$$

$$\mathbf{K}\mathbf{E}^{(1)} = \mathbf{E}^{(1)} + \frac{i}{\epsilon_0\omega}\mathbf{j}^{(1)}. \tag{4}$$

By eliminating the perturbed current density vector, $\mathbf{j}^{(1)}$ from the above definitions we get

$$K_{ij} = \delta_{ij} + \frac{i\sigma_{ij}}{\epsilon_0\omega}, \tag{5}$$

where δ_{ij} is Kronecker's delta representing the identity tensor. If we now recall two of Maxwell's linearized equations

$$\mathbf{k}\times\mathbf{E}^{(1)} = \omega\mathbf{B}^{(1)}, \tag{6}$$

$$i\mathbf{k}\times\mathbf{B}^{(1)} = \mu_0\mathbf{j}^{(1)} - i\mu_0\epsilon_0\omega\mathbf{E}^{(1)}, \tag{7}$$

and eliminate the perturbed magnetic field vector $\mathbf{B}^{(1)}$ from the second equation using the first, we obtain after dividing by k^2 and using Eq. (4),

$$N^2\left(\frac{\mathbf{k}\times(\mathbf{k}\times\mathbf{E}^{(1)})}{k^2} + \mathbf{K}\mathbf{E}^{(1)}\right) = 0. \tag{8}$$

The above equation can be written in the form of Eq. (1),

$$\mathbf{R}\mathbf{E}^{(1)} = 0, \tag{9}$$

where we identify **R** as the dispersion tensor whose elements can now be written in terms of those of the dielectric tensor or, more conveniently, through Eq. (5), in terms of those of the conductivity tensor

$$R_{ij} = N^2\left(\frac{k_i k_j}{k^2} - \delta_{ij}\right) + \delta_{ij} + \frac{i\sigma_{ij}}{\epsilon_0\omega}, \tag{10}$$

where

$$N \equiv \frac{ck}{\omega}, \tag{11}$$

is the index of refraction.

In order to arrive at the sought expressions for R_{ij} we shall invoke plasma kinetic theory to find a relation between the current density and the electric field which we shall put in the form of Eq. (3) thus allowing us, through Eq. (10), to write the dispersion tensor explicitly.[19]

C. Derivation of the perturbed distribution function

Our starting point for formulating a kinetic prescription relating the perturbed current density vector to the electric field is the Vlasov equation with the collisions represented by the Bhatnagar, Gross, and Krook (BGK) model,[20]

$$\frac{\partial f_s}{\partial t} + \mathbf{v}\cdot\nabla_{\mathbf{x}} f_s + \frac{q_s}{m_s}[\mathbf{E}(\mathbf{x},t) + \mathbf{v}\times\mathbf{B}]\cdot\nabla_{\mathbf{v}} f_s(\mathbf{x},\mathbf{v},t) = -\nu_s\left(f_s - \frac{n_s}{n_s^{(0)}} f_s^{(0)}\right), \tag{12}$$

where q_s, m_s, f_s, v_s are the charge, mass, velocity distribution function, and collision frequency of species *s*, respectively. We now linearize by assuming that all quantities with spatial and temporal dependences, **E**, **B**, f_s, **j** and the charge density ρ are perturbed about their steady-state values (superscripted with 0) by harmonic quantities (superscripted

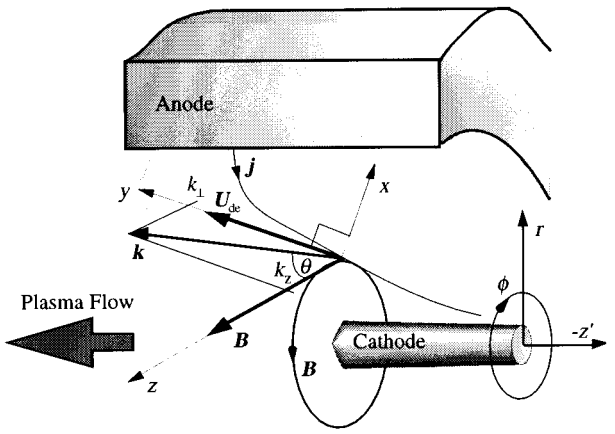

FIG. 1. The vectors **j**, **B**, **k** and $\mathbf{u_{de}}$ in the local Cartesian coordinate frame. Also shown is the accelerator's fixed cylindrical coordinate frame, $r-z'-\theta$.

with 1) so that for a generic quantity a we have $a=a^{(0)}+a^{(1)}$ and $|a^{(1)}/a^{(0)}|\ll 1$. After replacing the temporal and spatial differential operators by $-i\omega$ and $i\mathbf{k}$, respectively, the linearization of Eq. (12) results in the following expression for the perturbed distribution function:

$$-i(\omega+i\nu_s-\mathbf{k}\cdot\mathbf{v})f_s^{(1)}+\frac{q_s}{m_s}(\mathbf{v}\times\mathbf{B}^{(0)})\cdot\nabla_{\mathbf{v}}f_s^{(1)}$$
$$=-\frac{q_s}{m_s}(\mathbf{E}^{(1)}+\mathbf{v}\times\mathbf{B}^{(1)})\cdot\nabla_{\mathbf{v}}f_s^{(0)}+\nu_s\frac{n_s^{(1)}}{n_s^{(0)}}f_s^{(0)}. \tag{13}$$

If we choose to work with the cylindrical phase space coordinates, $v_\perp$, ϕ, v_z, with the magnetic field aligned with the z-axis, the above equation can be recast into a first order linear inhomogeneous differential equation in $f_s^{(1)}$ which can be integrated once to yield

$$f_s^{(1)}=\frac{1}{\Upsilon(\phi)\omega_{cs}}\int\Upsilon(\phi)\times\left\{\frac{q_s}{m_s}\left[\mathbf{E}^{(1)}+\frac{(\mathbf{v}\cdot\mathbf{E}^{(1)})\mathbf{k}-(\mathbf{k}\cdot\mathbf{v})\mathbf{E}^{(1)}}{\omega}\right]\cdot\nabla_{\mathbf{v}}f_s^{(0)}+\nu_s\frac{n_s^{(1)}}{n_s^{(0)}}f_s^{(0)}\right\}d\phi+C, \tag{14}$$

where the integrating factor $\Upsilon(\phi)$ can be written as

$$\Upsilon(\phi)=\exp\left[i\frac{\omega+i\nu_s-k_zv_z}{\omega_{cs}}\phi\right]\times\sum_{n=-\infty}^{\infty}i^nJ_n\left(\frac{k_\perp v_\perp}{\omega_{cs}}\right)e^{in\phi}, \tag{15}$$

where $J_n(a)$ is the Bessel function of integer order n and we have chosen, without any loss of generality, the wave vector to be in the $y-z$ plane as shown in Fig. 1, namely $\mathbf{k}=(0,k_\perp,k_z)$.

We now introduce the steady-state distribution function $f_s^{(0)}$. We choose to carry our derivation in the laboratory frame by allowing cross-field drifts in both the ion and electron distribution functions. For a cross-field drift in a homogeneous plasma the steady-state distribution function is a drifting Maxwellian

$$f_s^{(0)}(\mathbf{v})=\left(\frac{m_s}{2\pi T_s}\right)^{3/2}\times\exp\left[-\frac{m_s}{2T_s}(v_x^2+(v_y-u_{ds})^2+v_z^2)\right], \tag{16}$$

where u_{ds} and T_s are the cross-field drift velocity and temperature of species s in the laboratory frame. The drift velocity is taken to be aligned along the y-axis as shown in Fig. 1.

Upon substituting the above expression and Eq. (15) in Eq. (14), integrating over the azimuthal angle and using the following recursive relations:

$$J_{n-1}(a)+J_{n+1}(a)=2\frac{n}{a}J_n(a), \tag{17}$$

$$J_{n-1}(a)-J_{n+1}(a)=2J_n'(a), \tag{18}$$

where the prime denotes the derivative with respect to the argument, we obtain

$$f_s^{(1)}=\frac{iq_s}{\omega T_s}(\omega-k_\perp u_{ds})f_s^{(0)}\times\frac{e^{-in\phi}\Sigma_{m=-\infty}^{\infty}i^mJ_m(k_\perp v_\perp/\omega_{cs})e^{im\phi}}{\omega+i\nu_s+n\omega_{cs}-k_zv_z-k_\perp u_{ds}}\times\left\{\mathbf{C_n}\cdot\mathbf{E}^{(1)}+\nu_s\frac{n_s^{(1)}T_s}{n_s^{(0)}q_s}J_n\right\}, \tag{19}$$

where the vector of coefficients $\mathbf{C_n}$ is defined as

$$\mathbf{C_n}\equiv iv_\perp J_n'\hat{e}_x+\left(v_{ds}-\frac{n\omega_{cs}}{k_\perp}\right)J_n\hat{e}_y+v_zJ_n\hat{e}_z. \tag{20}$$

D. Switching to the potential formalism

We now switch from the electric field formalism exemplified in Eq. (1) to a formalism cast in terms of the electrostatic and electromagnetic potentials, Φ and $\mathbf{A}$ defined below. This has three advantages. The first advantage is a clear separation of electromagnetic and electrostatic effects in the dispersion tensor making it more natural to a discussion of electromagnetic correction to an electrostatic mode.[21] This will be especially advantageous in the context of the anomalous transport theory in Sec. III, where it will be insightful to separate the electrostatic and electromagnetic contributions to the anomalous heating and momentum exchange rates. The second advantage is the fact that, in the case where the ions are taken to be unmagnetized, their contribution to the dispersion tensor is much tidier mathematically than in the electric field formalism. Finally, the third advantage is that the effects of collisions on the purely electromagnetic modes can be simply prescribed in the potential formalism.

The electromagnetic potential $\mathbf{A}$ is defined by

$$\mathbf{B}=\nabla\times\mathbf{A}. \tag{21}$$

Any arbitrary choice of $\mathbf{A}$ of the form $\mathbf{A}+\nabla\psi$ (where ψ is single-valued) is, in general, possible. This ''arbitrariness of

gauge,'' as it is customarily called in electrodynamics, is most appropriately removed by imposing the Coulomb gauge $\nabla\cdot\mathbf{A}=0$. Rewriting the ''$\nabla\times\mathbf{E}$'' Maxwell equation using the above definition we get

$$\nabla\times\left(\mathbf{E}+\frac{\partial\mathbf{A}}{\partial t}\right)=0, \tag{22}$$

which implies that the quantity $(\mathbf{E}+\partial\mathbf{A}/\partial t)$ can be represented by a potential gradient $-\nabla\Phi$, and for linear harmonic perturbations we thus have

$$\mathbf{E}^{(1)}=i\omega\mathbf{A}^{(1)}-i\mathbf{k}\Phi^{(1)}. \tag{23}$$

Taking the divergence of the electric field, using the corresponding Maxwell equation and the Coulomb gauge we also get

$$\Phi^{(1)}=\frac{\rho^{(1)}}{\epsilon_0 k^2}. \tag{24}$$

Finally, upon substituting Eqs. (84) and (21) in Maxwell's ''$\nabla\times\mathbf{B}$'' equation, the following relation results:

$$\left(k^2-\frac{\omega^2}{c^2}\right)\mathbf{A}^{(1)}-\frac{\omega}{c^2}\mathbf{k}\Phi^{(1)}=\mu_0\mathbf{j}^{(1)}. \tag{25}$$

The above two equations become specified once expressions for the perturbed charge and current densities, $\rho^{(1)}$ and $\mathbf{j}^{(1)}$, are found in terms of $\mathbf{A}^{(1)}$ and $\Phi^{(1)}$. This will be done using the following moments:

$$\rho^{(1)}=\sum_s q_s\int f_s^{(1)}d^3\mathbf{v}, \tag{26}$$

$$\mathbf{j}^{(1)}=\sum_s q_s\int f_s^{(1)}\mathbf{v}d^3\mathbf{v}, \tag{27}$$

so that Eqs. (24) and (25) can be written as a set of three homogeneous equations in $\Phi^{(1)}$, $A_x^{(1)}$, and $A_z^{(1)}$ (and we have eliminated $A_y^{(1)}$ with the Coulomb gauge)

$$\begin{pmatrix} D_{11} & D_{12} & D_{13}\\ D_{21} & D_{22} & D_{23}\\ D_{31} & D_{32} & D_{33}\end{pmatrix}\begin{pmatrix}\Phi_{(1)}\\ A_x^{(1)}\\ A_z^{(1)}\end{pmatrix}=0. \tag{28}$$

The above matrix equation and the dispersion tensor D_{ij} are the analogs of Eq. (1) and the tensor R_{ij}, respectively, in the potential formalism.

The perturbed distribution function $f_s^{(1)}$ needed to take the moments in Eqs. (26) and (27) and close the system can now be rewritten in the potential formalism

$$\begin{aligned} f_s^{(1)}=&\frac{iq_s}{\omega T_s}(\omega-k_\perp u_{ds})f_s^{(0)}\\ &\times\frac{e^{-in\phi}\Sigma_{m=-\infty}^{\infty}i^m J_m(k_\perp v_\perp/\omega_{cs})e^{im\phi}}{\omega+i\nu_s+n\omega_{cs}-k_z v_z-k_\perp u_{ds}}\\ &\times\left\{\mathbf{C_n}\cdot(i\omega\mathbf{A}^{(1)}-i\mathbf{k}\Phi^{(1)})+\nu_s\frac{\mathbf{k}\cdot\mathbf{j}_s^{(1)}T_s}{\omega q_s^2 n_s^{(0)}}J_n\right\}, \end{aligned} \tag{29}$$

where we have also eliminated $n_s^{(1)}$ in favor of $j_s^{(1)}$ using

$$n_s^{(1)}=\frac{\mathbf{k}\cdot\mathbf{j}_s^{(1)}}{\omega q_s}, \tag{30}$$

which can be directly obtained by taking the divergence of Maxwell's ''$\nabla\times\mathbf{B}$'' equation.

E. The resulting dispersion tensor

The next step is to carry the velocity space integration required by the moments in Eqs. (26) and (27) using the above expression for $f_s^{(1)}$. The integration is carried in cylindrical velocity coordinates and thus takes the form

$$\int d^3\mathbf{v}=\int_0^\infty v_\perp dv_\perp\int_{-\infty}^{\infty}dv_z\int_0^{2\pi}d\phi. \tag{31}$$

After the integration over ϕ the parallel velocity integrals are of the form

$$\int_{-\infty}^{\infty}G(v_z)\frac{v_z^p}{\omega+i\nu_s+n\omega_{cs}-k_z v_z-k_\perp u_{ds}}dv_z, \tag{32}$$

where $p=0,1,2$. These integrals can be expressed as linear functions of the well known plasma dispersion function

$$Z(\zeta_s)\equiv\frac{1}{\sqrt{\pi}}\int_{-\infty}^{\infty}\frac{e^{-t^2}}{t-\zeta_s}dt, \tag{33}$$

and its derivative with respect to its argument. The integration over the perpendicular velocity transforms the Bessel functions into modified Bessel functions, $I_n(\mu_s)$ of the first kind and of integer order n with the argument being the square of the normalized perpendicular wavelength $\mu_s\equiv k_\perp^2 r_{cs}^2/2$.

After much tedious but straightforward algebra, where we use the following relations:

$$\frac{dZ}{d\zeta_s}=-2(1+\zeta_s Z), \tag{34}$$

$$\sum_{n=-\infty}^{\infty}nI_n(\mu_s)=0,\qquad\sum_{n=-\infty}^{\infty}I_n(\mu_s)=e^{\mu_s}, \tag{35}$$

$$\sum_{n=-\infty}^{\infty}n^2I_n(\mu_s)=\mu_s e^{\mu_s}, \tag{36}$$

assume the ions to be unmagnetized but keep in full their electromagnetic contribution (which has been demonstrated in Ref. 22 to be important) and neglect the ion collisions [since for the MPDT plasma, $\nu_i\ll\omega_{lh}<\nu_e$ (Refs. 6, 23)], the elements of the dispersion tensor D_{ij} can finally be written explicitly in terms of the wave and plasma parameters,

$$\begin{aligned} D_{11}=&1+\alpha_i(1+\zeta_i Z_i)\\ &+\alpha_e\left(\frac{1+\zeta_{e0}e^{-\mu_e}\Sigma_{n=-\infty}^{\infty}I_n Z_{en}}{1+i(\nu_e/k_z v_{te})e^{-\mu_e}\Sigma_{n=-\infty}^{\infty}I_n Z_{en}}\right), \end{aligned} \tag{37}$$

$$\begin{aligned} D_{12}=&-i\frac{\omega_{pe}^2}{\tilde{\omega}^2}\frac{k_z}{k}\zeta_{e0}\sqrt{2\mu_e}e^{-\mu_e}\\ &\times\sum_{n=-\infty}^{\infty}(I_n-I_n')(1+\tilde{\zeta}_{e0}Z_{en}), \end{aligned} \tag{38}$$

$$D_{13}=2\frac{\omega_{pe}^2}{\tilde{\omega}^2}\frac{k_z}{k}\zeta_{e0}e^{-\mu_e}\times\sum_{n=-\infty}^{\infty}I_n\left\{\vartheta_n^2 Z_{en}+\left[\left(\frac{u_{de}}{v_{te}}\right)^2\Big/\zeta_{e0}\right]+(1+\zeta_{en}Z_{en})\left(\vartheta_n\frac{k_\perp^2-k_z^2}{k_\perp k_z}-\zeta_{en}\right)\right\},\tag{39}$$

$$D_{22}=1-N^2+\frac{\omega_{pi}^2}{\omega^2}\zeta_i Z_i+\frac{\omega_{pe}^2}{\tilde{\omega}^2}\zeta_{e0}\mu_e e^{-\mu_e}\times\sum_{n=-\infty}^{\infty}\left[\frac{n^2}{\mu_e^2}I_n+2(I_n-I_n')\right]Z_{en},\tag{40}$$

$$D_{23}=-i\frac{\omega_{pe}^2}{\tilde{\omega}^2}\zeta_{e0}\sqrt{2\mu_e}e^{-u_e}\sum_{n=-\infty}^{\infty}(I_n-I_n')\times\left[1+\left(\frac{k_z}{k_\perp}\vartheta_n+\zeta_{en}\right)Z_{en}\right],\tag{41}$$

$$D_{33}=1-N^2+\frac{\omega_{pi}^2}{\omega^2}\zeta_i Z_i+2\frac{\omega_{pe}^2}{\tilde{\omega}^2}\frac{k_\perp^2}{k^2}\left[\left(\zeta_{e0}-\frac{k_z}{k_\perp}\frac{u_{de}}{v_{te}}\right)^2+\zeta_{e0}e^{-\mu_e}\sum_{n=-\infty}^{\infty}I_n Z_{en}\left(\frac{k_z}{k_\perp}\vartheta_n+\zeta_{en}\right)^2\right],\tag{42}$$

$$D_{21}=-D_{12},\quad D_{31}=\frac{k_\perp^2}{k^2}D_{13},\tag{43}$$

$$D_{32}=-\frac{k_\perp^2}{k^2}D_{23},\tag{44}$$

where we have used the following definitions:

$$\zeta_{en}\equiv\frac{\omega+n\omega_{ce}-k_\perp u_{de}+i\nu_e}{k_z v_{te}},\quad \zeta_i\equiv\frac{\omega-k_\perp u_{di}}{k v_{ti}},\tag{45}$$

$$\tilde{\omega}\equiv\omega+i\nu_e,\quad \tilde{\zeta}_{e0}\equiv\frac{\tilde{\omega}}{k_z v_{te}}=\zeta_{e0}+\frac{k_\perp}{k_z}\frac{u_{de}}{v_{te}},\tag{46}$$

$$\vartheta_n\equiv\frac{k_z}{k_\perp}(\zeta_{en}-\tilde{\zeta}_{e0}),\quad Z_{en}\equiv Z(\zeta_{en}),\quad I_n\equiv I_n(\mu_e),\tag{47}$$

and the thermal velocity, plasma frequency and cyclotron frequency of species s are, respectively, given by

$$v_{ts}=(2T_s/m_s)^{1/2},\quad \omega_{ps}\equiv\left(\frac{q_s^2 n_{0_s}}{\epsilon_0 m_s}\right)^{1/2};\quad \omega_{cs}\equiv\frac{q_s B_0}{m_s}.\tag{48}$$

It is also useful to note that the refraction index N appearing in the above dispersion tensor can be related to the plasma parameters through the following relation:

$$N^2\equiv\frac{c^2k^2}{\omega^2}=2\frac{\omega_{pi}^2}{\omega^2}\frac{\mu_e}{\beta_e}\frac{m_i}{m_e}\frac{k^2}{k_\perp^2},\tag{49}$$

where we have introduced β_s, the beta of species s, (s in the above equation is set to e for electrons) defined as the ratio of thermal pressure to magnetic pressure

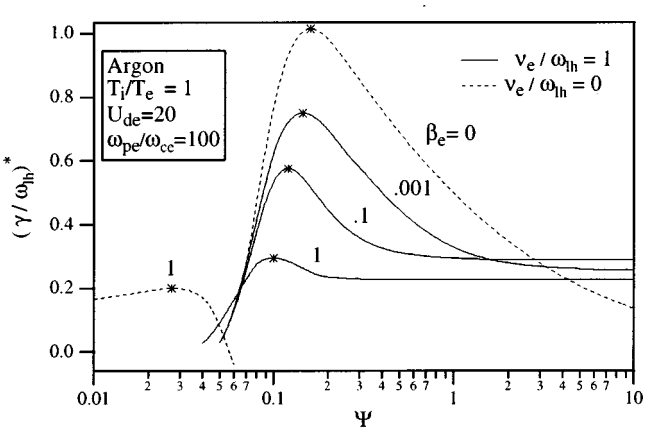

FIG. 2. Normalized temporal growth rates for collisional and collisionless unstable modes in argon as a function of the anisotropy parameter and the electron beta. The solutions are growth-maximized over wavelength. The stars on the curves denote the dominant (doubly-maximized) modes.

$$\beta_s\equiv\frac{n_s k T_s}{B_0^2/2\mu_0}.\tag{50}$$

Finally, by writing

$$\frac{\omega_{pi}^2}{\omega^2}=\frac{\alpha_i}{2\zeta_i^2}\quad\text{and}\quad\frac{\omega_{pe}^2}{\omega^2}=\frac{k^2}{k_\perp^2}\frac{\alpha_e}{2\zeta_e^2},\tag{51}$$

where

$$\alpha_s\equiv\frac{k_\perp^2\omega_{ps}^2}{k^2\omega_{cs}^2\mu_s}=\frac{2\omega_{ps}^2}{k^2 v_{ts}^2}=\frac{1}{k^2\lambda_{ds}^2},\tag{52}$$

(λ_{ds} is the Debye length for species s) and by defining a nondimensional parameter Ψ related to the propagation angle θ (see Fig. 1) scaled by the mass ratio

$$\Psi\equiv(m_e/m_i)^{1/2}\frac{k}{k_z}=\frac{(m_e/m_i)^{1/2}}{\cos\theta},\tag{53}$$

it can be verified that the following set of seven dimensionless parameters

$$\frac{T_i}{T_e},\quad\frac{u_{de}}{v_{ti}},\quad\Psi,\quad\beta_e,\quad\frac{\omega_{pe}}{\omega_{ce}},\quad\frac{m_i}{m_e},\quad\frac{\nu_e}{\omega_{lh}},\tag{54}$$

completely specify the problem such that, for a given real wave number, kr_{ce} (where r_{ce} is the electron cyclotron radius) we seek the roots, ω/ω_{lh} and γ/ω_{lh} of the dispersion relation[24]

$$\det|D_{ij}|=0.\tag{55}$$

It is also worth mentioning that the electrostatic dispersion relation (obtained in the limit $\beta\to0$) is simply $D_{11}=0$.

Dominant modes. We now show the results of calculations using the above dispersion relation to illustrate some of the characteristics of the unstable modes and their parametric dependencies. The solutions shown in Fig. 2 have been growth-maximized over wavelength and thus represent the dominant modes. The parameter $U_{\rm de}$ represents the ratio $u_{\rm de}/v_{ti}$.

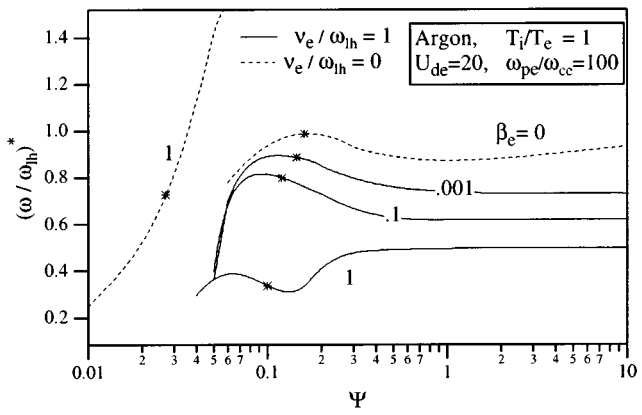

FIG. 3. Normalized frequencies for collisional and collisionless unstable modes in argon as a function of the anisotropy parameter and the electron beta. The solutions are growth-maximized over wavelength. The stars on the curves denote the dominant (doubly-maximized) modes.

The enhancement of electromagnetic coupling with increasing β_e results in a damping of the dominant mode as can be seen from that figure.

The damping is not drastic since more than a three order of magnitude increase in β_e corresponds to only a factor of 2 decrease in the growth rate of the dominant modes. The instability not only persists under finite-beta effects but, as can be seen from the $\beta_e=1$ (and $\nu_e/\omega_{lh}=1$) curve in that figure, encompasses a somewhat wider range of propagation angles than it did for the purely electrostatic case.

The finite-beta effects therefore are *not* globally stabilizing as was previously speculated,[15–17,14] even for drift velocities exceeding the Alfvén velocity, but rather result in the excitation of finite-growth modes with mixed polarization. This corroborates the findings of Refs. 25, 18, 26 and extends the validity of their argument to the collisional case.

The collisionless solutions are also shown in the same figure for both the $\beta_e=0$ (electrostatic) and $\beta_e=1$ cases. It is obvious that the effects of finite beta are qualitatively different for the collisionless and collisional dominated cases.

In the absence of collisions the electromagnetic effects result in a shifting of the instability to more oblique propagation. For argon with $\beta_e=1$ and $U_{de}=20$, for instance, the dominant mode shifts by more than 6° towards the magnetic field vector from the orientation of the purely electrostatic dominant mode. The shift is more pronounced for lighter atoms (approaching 50° for hydrogen). This effect was first discovered by Wu *et al.*[26] who noted that electromagnetic effects actually stabilize nearly perpendicular waves and destabilize more oblique ones. Since many of the preceding studies that addressed the finite-beta effects on the electrostatic modified two-stream instability focused on either perpendicular or nearly perpendicular propagation, electromagnetic effects (which become important when $u_{de}>v_A$) were generally thought to be stabilizing.

The frequencies of the unstable modes, growth-maximized over wavelength, are of the order of the lower hybrid frequency as shown in Fig. 3. The dotted curves represent the collisionless case that corresponds to the generalized lower hybrid drift instability (GLHDI) previously discussed in Refs. 15–17, 26.

Consistent with the above results, we find that the angular dependence of the frequencies of the collisional mixed polarization modes resembles more that of the electrostatic collisionless modes than that of the collisionless mixed polarization modes. This indicates that unstable electrostatic oscillations couple differently with electromagnetic oscillations when collisions are important.

We conclude from the above linear stability analysis that plasma parameters typical of the collisional and transverse current-carrying plasma of a Lorentz force plasma accelerator, $10\leqslant U_{de}\leqslant 100$, $T_i/T_e=\mathcal{O}(1)$, $\nu_s<\omega_{ce}$ and $\beta\sim\mathcal{O}(1)$, a mixed polarization mode can be easily driven unstable by the cross-field current. The stability boundaries are broad enough and the evolution time scales are fast enough that the energy associated with the unstable oscillating electric and magnetic field spectra may be expected to significantly alter basic transport processes as will be seen next.

III. WEAK TURBULENCE KINETIC FORMALISM FOR ANOMALOUS TRANSPORT

The kinetic theory of weak turbulence was first developed by Vedenov, Velikhov, and Sagdeev[27] (1961), as well as Drummond, Pines and Rosenbluth[28] (1962). A good treatment is given by Galeev and Sagdeev in Ref. 29 (1982).

The use of weak turbulence theory is generally justified when

$$\frac{\mathcal{E}_t}{\Sigma_s n_s T_s}\ll 1. \tag{56}$$

We can relate $\mathcal{E}_t/n_0T_i$ to the experimentally measurable density fluctuation $\tilde{n}/n_0$, where the tilde denotes a fluctuating quantity by noting that $\tilde{n}/n_0\approx e\tilde{\phi}/T_e$ and $e\tilde{\phi}\approx e\tilde{E}/k$,

$$\frac{\mathcal{E}_t}{n_0T_i}\approx\frac{T_e}{T_i}\frac{(kr_{ce})^2}{4}\left(\left.\frac{\tilde{n}}{n_0}\right|_{\rm rms}\right)^2. \tag{57}$$

Experimental evidence of turbulent fluctuations caused by cross-field current-driven instabilities was recently found in the low-power steady-state MPDT plasma at various conditions and locations in the plume.[7] These measured turbulent fluctuations had most of their power in the lower hybrid mode with some power appearing sometimes in the electron cyclotron harmonics. Measured values of $(\tilde{n}/n_0)_{\rm rms}$ when such turbulence was observed were on the order of 0.1 with magnitudes ranging between 0.05 and 0.7. For these values, with $1\leqslant T_i/T_e\leqslant 6$, $\mathcal{E}_t=\epsilon_0|\tilde{E}_k|^2/2$ and assuming the doubly growth-maximized $(kr_{ce})^{**}\approx 0.1$, we obtain from Eq. (57) an estimate for $\mathcal{E}_t/n_0T_i$ ranging between 10^{-3} and 10^{-6} implying that the weak turbulence assumption is generally valid.

A. Governing equations: The moment-generating equation

In this subsection we present an outline of the derivation of the general form of fluid-like equations governing the evolution of macroscopic quantities under the conditions of

weak turbulence. Detailed discussions of such a derivation have already been presented in numerous articles (see Refs. 30, 31, for instance, for a tutorial review). We do this in preparation to our derivation of anomalous transport presented in the following sections.

We should mention at the outset that our interest lies not in the evolution equation itself but rather in its use as a moment-generating equation. Therefore, for the sake of simplicity and in order to keep a connection with the literature, we shall neglect collisions in the kinetic evolution equation. The effects of collisions will be reintroduced later when we use the explicit form of the dispersion tensor elements.

The underlying idea[32] is to consider the distribution function of the s species, f_s, as the sum of a slowly varying ensemble-average part and a rapidly varying fluctuating part

$$f_s(\mathbf{x},\mathbf{v},t)=F_s(\mathbf{v},t)+\tilde{f}_s(\mathbf{x},\mathbf{v},t), \tag{58}$$

where $F_s(\mathbf{v},t)=\langle f_s(\mathbf{x},\mathbf{v},t)\rangle$ and $\langle\ \rangle$ denotes an ensemble-average while the tilde denotes a quantity fluctuating due to the effects of unstable waves. When similar partitions are effected on the electric and magnetic field vectors, the kinetic (Vlasov) equation for a spatially uniform equilibrium yields

$$\frac{\partial F_s}{\partial t}-\omega_{cs}\frac{\partial F_s}{\partial\phi}+\frac{q_s}{m_s}[\tilde{\mathbf{E}}+\mathbf{v}\times\tilde{\mathbf{B}}]\cdot\nabla_v F_s = -\left(\frac{\partial\tilde{f}_s}{\partial t}+\mathbf{v}\cdot\nabla\tilde{f}_s-\omega_{cs}\frac{\partial\tilde{f}_s}{\partial\phi}+\frac{q_s}{m_s}[\tilde{\mathbf{E}}+\mathbf{v}\times\tilde{\mathbf{B}}]\cdot\nabla_v\tilde{f}_s\right), \tag{59}$$

where, like in Sec. II we have chosen to work with the cylindrical phase space coordinates $v_\perp$, ϕ, v_z. Taking the ensemble-average of the above equation, while noting that $\langle\tilde{f}_s\rangle=0$, results in

$$\frac{\partial F_s}{\partial t}-\omega_{cs}\frac{\partial F_s}{\partial\phi}=\left(\frac{\partial F_s}{\partial t}\right)_{AN}, \tag{60}$$

where the right-hand side represents the anomalous contribution that is the response of the average distribution function to the microturbulent fluctuations and can be written explicitly as

$$\left(\frac{\partial F_s}{\partial t}\right)_{AN}=\left\langle-\frac{q_s}{m_s}[\tilde{\mathbf{E}}+\mathbf{v}\times\tilde{\mathbf{B}}]\cdot\nabla_v\tilde{f}_s\right\rangle. \tag{61}$$

By subtracting Eq. (61) from Eq. (59) and, in the spirit of weak turbulence theory, neglecting all terms that are quadratic in the fluctuation amplitude (which is tantamount to the neglect of *nonlinear* wave–particle and wave–wave interactions) the following governing equation is obtained for a weakly turbulent plasma:

$$\frac{\partial\tilde{f}_s}{\partial t}+\mathbf{v}\cdot\nabla\tilde{f}_s-\omega_{cs}\frac{\partial\tilde{f}_s}{\partial\phi}=-\frac{q_s}{m_s}[\tilde{\mathbf{E}}+\mathbf{v}\times\tilde{\mathbf{B}}]\cdot\nabla_v F_s. \tag{62}$$

The standard procedure in weak turbulence theory (expounded in Ref. 32 for instance) is to solve Eq. (62) along with Maxwell's equations for $\tilde{\mathbf{E}}$, $\tilde{\mathbf{B}}$, and $\tilde{f}_s$ then substitute the result into Eq. (60) to obtain the evolution of F_s in the presence of microturbulence. We shall not, however, need to do all that for our particular problem of deriving expressions for the momentum and energy exchange rates. Such expressions can be arrived at by taking moments of the governing equation [Eq. (60)] as outlined below.

B. Evolution of average macroscopic properties under microturbulence

To obtain the macroscopic evolution equations we take moments of Eq. (60), i.e., we multiply the equation by the generic quantity of transport Θ (which could represent mass, momentum or energy) and integrate over velocity space to get

$$\frac{\partial}{\partial t}\int\Theta F_s d\mathbf{v}-q_s m_s\int(\mathbf{v}\times\mathbf{B}_0\cdot\nabla_v\Theta)F_s d\mathbf{v} = \frac{q_s}{m_s}\left\langle\int[(\tilde{\mathbf{E}}+\mathbf{v}\times\tilde{\mathbf{B}})\cdot\nabla_v\Theta]\tilde{f}_s d\mathbf{v}\right\rangle, \tag{63}$$

where we have used integration by parts in order to move the distribution functions outside the operators. Taking successive moments of Eq. (60) is equivalent to substituting $\Theta=1$, $\mathbf{v}$, $\mathbf{vv}$ (for mass, momentum and energy, respectively) in Eq. (63) and integrating over $\mathbf{v}$-space. This yields

$$\frac{\partial\langle n_s\rangle}{\partial t}=0, \tag{64}$$

$$\frac{\partial\langle\mathbf{\Gamma}_s\rangle}{\partial t}+(\omega_{cs}\mathbf{e}_z)\times\langle\mathbf{\Gamma}_s\rangle=\frac{q_s}{m_s}\langle\tilde{\mathbf{E}}\tilde{n}_s+\tilde{\mathbf{\Gamma}}_s\times\tilde{\mathbf{B}}\rangle, \tag{65}$$

$$\frac{\partial\langle\mathbf{W}_s\rangle}{\partial t}+2(\omega_{cs}\mathbf{e}_z)\times\langle\mathbf{W}_s\rangle=2\frac{q_s}{m_s}\langle\tilde{\mathbf{E}}\tilde{\mathbf{\Gamma}}_s+\tilde{\mathbf{W}}_s\times\tilde{\mathbf{B}}\rangle, \tag{66}$$

where $\mathbf{e}_z$ is the unit vector along the z-axis, and we have used the following definitions:

$$n_s=\int f_s d\mathbf{v}, \tag{67}$$

$$\mathbf{\Gamma}_s=n_s\mathbf{v}_{ds}=\int\mathbf{v}f_s d\mathbf{v}, \tag{68}$$

$$\mathbf{W}_s=m_s\int\mathbf{vv}f_s d\mathbf{v}, \tag{69}$$

for the average number density, the particle flux density, and the kinetic energy density tensor, respectively (with $\mathbf{v}_{ds}$ as the drift velocity vector of species s).

IV. MOMENTUM EXCHANGE AND HEATING RATES

We now proceed to define and derive explicit relations for the anomalous rates of interest.

The right-hand side of Eq. (65) represents the rate of momentum exchange $(\partial\mathbf{P}_s/\partial t)_{AN}$ (where the momentum density vector is $\mathbf{P}_s=m_s\mathbf{\Gamma}_s$) between the particles and the fluctuating fields. Since we shall be interested in the momentum exchange along the drift velocity vector, we write

$$\left(\frac{\partial\mathbf{P}_s}{\partial t}\right)_{AN}\cdot\mathbf{v}_{ds}=-(\nu_s^p)_{AN}\mathbf{P}_s\cdot\mathbf{v}_{ds}, \tag{70}$$

where we have defined $(\nu_s^p)_{AN}$ as the effective anomalous momentum exchange rate (or frequency) between species s and the fluctuating fields. Using the explicit expression for $(\partial \mathbf{P}_s/\partial t)_{AN}$ from Eq. (65) in the above equation we obtain

$$(\nu_s^p)_{AN} = -\frac{q_s}{n_s m_s v_{ds}} \left\langle \frac{\tilde{\mathbf{E}} \cdot \mathbf{v}_{ds} \tilde{n}_s}{v_{ds}} + \frac{\mathbf{v}_{ds} \cdot (\tilde{\mathbf{\Gamma}}_s \times \tilde{\mathbf{B}})}{v_{ds}} \right\rangle, \tag{71}$$

where, unlike most derivations in the literature, we are retaining the full electromagnetic character of the microturbulence.

We now specialize the above expression for our particular problem according to the MPDT configuration shown in Fig. 1.

We thus obtain the effective anomalous momentum exchange rate for electrons along the current after setting $s=e$, staying in the ion reference frame and aligning the relative drift u_{de} along the y-axis,

$$(\nu_e^p)_{AN} = \frac{e}{n_0 m_e u_{de}} \langle \tilde{E}_y \tilde{n}_e + n_0 \tilde{u}_{de_z} \tilde{B}_x - n_0 \tilde{u}_{de_x} \tilde{B}_z \rangle, \tag{72}$$

where we have used the relation $\tilde{\Gamma}_s = \tilde{n}_s \mathbf{v}_{ds} + n_0 \tilde{\mathbf{v}}_{ds}$.

The frequency $(\nu_e^p)_{AN}$ can be thought of as an effective ''collision'' frequency between the electrons and the fluctuating fields and can thus be associated with a resistivity called ''anomalous resistivity'' the same way that the coulomb collision frequency ν_{ei} is associated with the classical Spitzer resistivity. By analogy the anomalous resistivity $(\eta)_{AN}$ is proportional to $(\nu_e^p)_{AN}$ and is given by

$$(\eta)_{AN} = \frac{m_e (\nu_e^p)_{AN}}{n_0 e^2}. \tag{73}$$

The effective collision frequency $(\nu_e^p)_{AN}$ is therefore a direct measure of anomalous resistivity.

Similarly, for the temperature

$$T_s = \frac{m_s}{3 n_s} \int (\mathbf{v} - \mathbf{v}_{ds})^2 f_s d\mathbf{v} \tag{74}$$

we define a heating rate for species s by

$$\nu_s^T \equiv \frac{1}{T_s} \frac{\partial T_s}{\partial t}, \tag{75}$$

and obtain, after combining Eqs. (65) and (66) and specializing for the MPDT configuration,

$$(\nu_i^T)_{AN} = \frac{2e}{3 n_0 T_i} \langle n_0 \tilde{\mathbf{E}} \cdot \tilde{\mathbf{u}}_{di} \rangle, \tag{76}$$

for the ions and

$$(\nu_e^T)_{AN} = \frac{-2e}{3 n_0 T_e} \langle n_0 \tilde{\mathbf{E}} \cdot \tilde{\mathbf{u}}_{de} - n_0 u_{de} (\tilde{u}_{de_z} \tilde{B}_x - \tilde{u}_{de_x} \tilde{B}_z) \rangle, \tag{77}$$

for the electrons.

Equations (72), (76), and (77) will be the focus of our remaining analysis and calculations.

In order to proceed with more useful forms for these expressions we need to eliminate the fluctuating density, velocity and magnetic field in favor of the fluctuating electric field. For this purpose we invoke, in the spirit of a quasilinear description, relations between the fluctuating quantities and the fluctuating electric field that follow those of their linearly oscillating counterparts. From a generalized Ohm's law we can write for species s,

$$\tilde{\mathbf{j}}_{s_k} = -i \epsilon_0 \omega \mathbf{R}^{(s)} \tilde{\mathbf{E}}_k, \tag{78}$$

(where $\mathbf{j}$ is the current density, $\mathbf{R}^{(s)}$ is the dispersion tensor of species s and ω is the wave frequency) which, combined with the continuity relation,

$$n_s^{(1)} = \frac{\mathbf{k} \cdot \mathbf{j}_s^{(1)}}{\omega q_s}, \tag{79}$$

gives a useful expression for the fluctuating density of species s

$$\tilde{n}_{s_k} = \frac{\mathbf{k} \cdot \tilde{\mathbf{j}}_s}{\omega q_s} = -i \frac{\epsilon_0}{q_s} \sum_l \; k_l \sum_m \; R_{lm}^{(s)} \tilde{E}_{m_k}, \tag{80}$$

where the subscript k is a reminder that these relations are for the spectrally resolved (i.e., Fourier transformed) fluctuations. In this expression, $R_{lm}^{(s)}$ are the elements of the tensor representing the dielectric response of species s and can be readily obtained from Eqs. (37)–(44) through transformations that will be described further below.

In a similar fashion we can derive an expression for $\tilde{\mathbf{u}}_{ds}$ from the following relation:

$$\tilde{\mathbf{j}}_s = q_s (n_0 \tilde{\mathbf{u}}_{ds} + \tilde{n}_s \mathbf{u}_{ds}), \tag{81}$$

and Eq. (80), yielding

$$\tilde{\mathbf{u}}_{s_k} = -\frac{i \epsilon_0 \omega \mathbf{R}^{(s)} \tilde{\mathbf{E}}_k}{q_s n_0} + \left[i \frac{\epsilon_0}{q_s n_0} \mathbf{k} \cdot (\mathbf{R}^{(s)} \tilde{\mathbf{E}}_k) \right] \mathbf{u}_{ds}. \tag{82}$$

We shall not need to worry about the second term on the right-hand side of the above equation in the context of the MPDT configuration shown in Fig. 1, because this term vanishes for the ions ($\mathbf{u}_{di}=0$, having chosen to stay in the ion rest frame) and for the electrons it is also zero for the components that figure in Eqs. (72) and (77) (i.e., the x and z components) so that we are left with

$$\tilde{u}_{ds_{l_k}} = -i \frac{\epsilon_0}{q_s n_0} \omega \sum_m \; R_{lm}^{(s)} \tilde{E}_{m_k}, \tag{83}$$

where $l=x,z$ for $s=e$; and $l=x,y,z$ for $s=i$.

Having related the fluctuating density and velocity to the fluctuating electric field we need to do the same for $\tilde{\mathbf{B}}$. To this end, the following equation

$$\tilde{\mathbf{E}} = i \omega \tilde{\mathbf{A}} - i \mathbf{k} \tilde{\Phi}, \tag{84}$$

gives, for our particular configuration,

$$\tilde{E}_{x_k} = i \omega \tilde{A}_{x_k}, \tag{85}$$

$$\tilde{E}_{y_k} = -i k_\perp \tilde{\Phi}_k - i \omega \frac{k_z}{k_\perp} \tilde{A}_{z_k}, \tag{86}$$

$$\tilde{E}_{z_k} = -i k_z \tilde{\Phi}_k + i \omega \tilde{A}_{z_k}. \tag{87}$$

Furthermore, combining the above equations with the definition of the electromagnetic potential, Eq. (21), and Coulomb's gauge, yields the desired relations

$$\tilde{B}_{x_k}=\frac{1}{\omega}(k_\perp \tilde{E}_{z_k}-k_z\tilde{E}_{y_k}), \tag{88}$$

$$\tilde{B}_{y_k}=\frac{k_z}{\omega}\tilde{E}_{x_k}, \tag{89}$$

$$\tilde{B}_{z_k}=-\frac{k_\perp}{\omega}\tilde{E}_{x_k}. \tag{90}$$

We are now in a position to evaluate the terms of Eqs. (72), (77), and (76) by carrying the ensemble-averages using the random phase approximation (which is a standard technique of statistical physics commonly used in the spectral resolution of fluctuations, see Ref. 33, pp. 371–373, for instance). For the first term in Eq. (72) using Eq. (80) we have,

$$\langle \tilde{E}_y\tilde{n}_e\rangle=\left\langle \int\int \frac{i\epsilon_0}{e}\sum_l k_l \sum R_{lm}^{(e)} \times \tilde{E}_{m_k}\tilde{E}_{y'_k}e^{i(\mathbf{k}\cdot\mathbf{x}+\mathbf{k}'\cdot\mathbf{x})}d\mathbf{k}\mathbf{k}'\right\rangle, \tag{91}$$

which yields, under the assumption of random phase,

$$\langle \tilde{E}_y\tilde{n}_e\rangle=-\frac{\epsilon_0}{e}\int \Im\left\{\sum_l k_l\sum_m R_{lm}^{(e)}\tilde{E}_m\tilde{E}_y\right\}d\mathbf{k}, \tag{92}$$

where $\Im\{\ \}$ denotes the imaginary part of a complex quantity and, for the sake of simplicity, we have dropped the subscript k from the fluctuating quantities. Similarly, we find for the other two terms in Eq. (72),

$$\langle \tilde{u}_{de_z}\tilde{B}_x\rangle=-\frac{\epsilon_0}{e}\int \Im\left\{\left(\sum_m R_{zm}^{(e)}\tilde{E}_m\right) \times(k_\perp\tilde{E}_z-k_z\tilde{E}_y)\right\}d\mathbf{k}, \tag{93}$$

$$\langle \tilde{u}_{de_x}\tilde{B}_z\rangle=\frac{\epsilon_0}{e}\int \Im\left\{\left(\sum_m R_{xm}^{(e)}\tilde{E}_m\right)k_\perp\tilde{E}_x\right\}d\mathbf{k}. \tag{94}$$

If we now substitute the above three equations in Eq. (72), expand and collect the terms in the summations while taking advantage of the following symmetry properties of the dispersion tensor:

$$R_{xy}^{(s)}=-R_{xy}^{(s)},\quad R_{xz}^{(s)}=-R_{zx}^{(s)},\quad R_{yz}^{(s)}=R_{zy}^{(s)}, \tag{95}$$

we arrive at

$$(\nu_e^p)_{AN}=-\frac{\epsilon_0}{u_{de}m_en_e}\int \Im\left\{k_\perp\left[\left(\sum_l R_{ll}^{(e)}|\tilde{E}_l|^2\right) +2R_{yz}^{(e)}|\tilde{E}_y\tilde{E}_z|\right]\right\}d\mathbf{k}. \tag{96}$$

We shall find it convenient, for our particular instability, to cast the the above expression in terms of the spectrally resolved fluctuating field energy density in the perpendicular direction, $\mathcal{E}_{k_\perp}$. This can be done by using the following relations obtained from Eq. (95) and Eq. (9) to yield

$$A\equiv\frac{\tilde{E}_x}{\tilde{E}_y}=\frac{R_{yy}R_{xz}-R_{xy}R_{yz}}{R_{xy}R_{xz}+R_{xx}R_{yz}}, \tag{97}$$

$$B\equiv\frac{\tilde{E}_z}{\tilde{E}_y}=-\frac{R_{xy}R_{xz}-R_{xx}R_{yz}}{R_{xx}R_{zz}+R_{xz}R_{xz}} \tag{98}$$

(where each element R_{lm} is the sum of the corresponding contributions from the electrons, ions and vacuum) to eliminate $\tilde{E}_x$ and $\tilde{E}_z$ and give

$$(\nu_e^p)_{AN}=-\frac{2}{u_{de}m_en_e}\int \mathcal{E}_{k_\perp}k_\perp\Im\{R_{xx}^{(e)}A^2+R_{yy}^{(e)}+R_{zz}^{(e)}B^2 +2R_{yz}^{(e)}B\}d\mathbf{k}. \tag{99}$$

We have carried out the derivation above under the electric field formalism where the relevant dispersion tensor is **R** [see Eq. (9)]. The dispersion tensor **D** that we derived explicitly in Sec. II, however, was obtained under the potential formalism. As stated in that section, switching to the potential formalism has some advantages. In the context of anomalous transport, the potential formalism allows a more physical insight by expressing the momentum exchange and heating rates in terms of an electrostatic contribution plus a finite-beta correction. The results obtained so far can readily be recast in terms of the elements D_{lm} of Eqs. (37)–(44), through the following linear transformations obtained from combining Eqs. (9), (85), (86), and (87),

$$R_{xx}=D_{22}, \tag{100}$$

$$R_{xy}=-R_{yx}=\frac{k_\perp}{k}\left(\frac{k_z}{k}D_{23}-D_{12}\right), \tag{101}$$

$$R_{xz}=-R_{zx}=-\frac{k_\perp^2}{k^2}D_{23}-\frac{k_z}{k}D_{12}, \tag{102}$$

$$R_{yy}=\frac{k_\perp^2}{k^2}\left(D_{11}+2\frac{k_z}{k}D_{13}\right)+\frac{k_z^2}{k^2}D_{33}, \tag{103}$$

$$R_{yz}=R_{zy}=\frac{k_\perp}{k}\left[\frac{k_z^2}{k^2}-\frac{k_\perp^2}{k^2}\right]D_{13}\ \text{nonumber} \tag{104}$$

$$+\frac{k_\perp k_z}{k^2}(D_{11}-D_{33}), \tag{105}$$

$$R_{zz}=\frac{k_\perp^2}{k^2}D_{33}+\frac{k_z^2}{k^2}D_{11}-2\frac{k_\perp^2}{k^2}\frac{k_z}{k}D_{13}. \tag{106}$$

We also need to separate the contributions of electrons, ions and vacuum in the dispersion tensor, which can be done following

$$D_{lm}^{(e)}=D_{lm}-D_{lm}^{(0)}-D_{lm}^{(i)}, \tag{107}$$

where subscripts l and m cover the indices 1, 2, and 3 and where the superscript (0) denotes the contribution of vacuum. The elements $D_{lm}^{(0)}$ and $D_{lm}^{(i)}$ are given by

$$D_{11}^{(0)}=1, \quad D_{22}^{(0)}=D_{33}^{(0)}=1-N^2, \quad D_{12}^{(0)}=D_{13}^{(0)}=D_{23}^{(0)}=0, \tag{108}$$

and

$$D_{11}^{(i)}=\frac{2\omega_{pi}^2}{k^2 v_{tli}^2}(1+\zeta_i Z_i), \tag{109}$$

$$D_{22}^{(i)}=D_{33}^{(i)}=\frac{\omega_{pi}^2}{\omega^2}\zeta_i Z_i, \tag{110}$$

$$D_{12}^{(i)}=D_{13}^{(i)}=D_{23}^{(i)}=0. \tag{111}$$

When the above transformations [Eqs. (100)–(111)] are used in Eq. (99) to eliminate $R_{lm}^{(e)}$ in favor of $D_{lm}^{(e)}$, we finally obtain after some straightforward algebra

$$\begin{aligned}(\nu_e^p)_{AN}=&[(\nu_e^p)_{AN}]_L-\frac{2}{u_{de}m_e n_e}\int \mathcal{E}_{k_\perp}k_\perp \\ &\times\Im\left\{D_{11}^{(e)}\left[B^2\frac{k_z^2}{k^2}-\frac{k_z^2}{k^2}+2B\frac{k_\perp k_z}{k^2}\right]+D_{22}^{(e)}A^2\right. \\ &+D_{33}^{(e)}\left[\frac{k_z^2}{k^2}+\frac{k_\perp^2}{k^2}B^2-2B\frac{k_\perp k_z}{k^2}\right]+2D_{13}^{(e)} \\ &\left.\times\left[B\frac{k_\perp}{k}\left(\frac{k_z^2}{k^2}-\frac{k_\perp^2}{k^2}\right)-\frac{k_\perp^2 k_z^2}{k^4}B^2+\frac{k_\perp^2 k_z}{k^3}\right]\right\}d\mathbf{k},\end{aligned} \tag{112}$$

where $[(\nu_e^p)_{AN}]_L$ is the well-known electrostatic (longitudinal) contribution to the anomalous electron momentum exchange rate

$$[(\nu_e^p)_{AN}]_L=-\frac{2}{u_{de}m_e n_e}\int \mathcal{E}_{k_\perp}k_\perp\Im\{\chi_e\}d\mathbf{k}, \tag{113}$$

and $\chi_e=D_{11}^{(e)}$ is the electrostatic susceptibility of the electrons. In the electrostatic limit ($\beta\to 0$) it can be verified that the integrand in Eq. (112) vanishes so that we are left with $(\nu_e^p)_{AN}\to[(\nu_e^p)_{AN}]_L$ and

$$\Im\{\chi_e\}=\Im\{D_{11}^{(e)}\}=\Im\{-D_{11}^{(i)}\}=\Im\{-\chi_i\}. \tag{114}$$

We shall demonstrate through the calculations of Sec. VI that the transverse (electromagnetic) or finite-beta correction to $(\nu_p^e)_{AN}$ in Eq. (112) can be substantial, especially for a finite-beta plasma like that of the MPDT.

Equations (99) and (112) are equivalent but, for the present analytical discussion, we prefer from here on to use the former (i.e., the electric field formalism) because the resulting expressions are more compact. For our numerical calculations we shall apply the transformations in Eqs. (100)–(111) in order to obtain the **R** tensor from the **D** tensor derived in Sec. II E.

It is convenient to express $(\nu_e^p)_{AN}$ in units of a natural frequency. We choose, as we did in Sec. II, the lower hybrid frequency, $\omega_{lh}\simeq\sqrt{\omega_{ci}\omega_{ce}}$, and normalize Eq. (99) to get

$$\begin{aligned}\frac{(\nu_e^p)_{AN}}{\omega_{lh}}=&-\frac{v_{ti}}{u_{de}}\left(\frac{T_i}{T_e}\right)^{1/2}\frac{m_i}{m_e}\int\frac{\mathcal{E}_{k_\perp}}{n_0T_i} \\ &\times\Im\{k_\perp r_{ce}[R_{xx}^{(e)}A^2+R_{yy}^{(e)}+R_{zz}^{(e)}B^2 \\ &+2R_{yz}^{(e)}B]\}d\mathbf{k}.\end{aligned} \tag{115}$$

We have focused, above, on the anomalous electron momentum exchange rate. Similar derivations, with no conceptual difference, start from Eqs. (76) and (82) and lead to the following expressions for the ion and electron heating rates $(\nu_i^T)_{AN}$ and $(\nu_e^T)_{AN}$:

$$\begin{aligned}\frac{(\nu_i^T)_{AN}}{\omega_{lh}}=&\frac{4}{3}\int\frac{\mathcal{E}_{k_\perp}}{n_0T_i}\Im\left\{\frac{\omega}{\omega_{lh}}[R_{xx}^{(i)}A^2+R_{yy}^{(i)}+R_{zz}^{(i)}B^2\right. \\ &\left.+2R_{yz}^{(i)}B]\right\}d\mathbf{k},\end{aligned} \tag{116}$$

$$\begin{aligned}\frac{(\nu_e^T)_{AN}}{\omega_{lh}}=&\frac{4}{3}\frac{T_i}{T_e}\int\frac{\mathcal{E}_{k_\perp}}{n_0T_i}\Im\left\{\left[\frac{\omega}{\omega_{lh}}-k_\perp r_{ce}\left(\frac{T_i}{T_e}\right)^{1/2}\frac{u_{de}}{v_{ti}}\right]\right. \\ &\times[R_{xx}^{(e)}A^2+R_{yz}^{(e)}B+R_{zz}^{(e)}B^2]+\frac{k_z}{k}\frac{u_{de}}{v_{ti}}k_\perp r_{ce}\left(\frac{T_i}{T_e}\right)^{1/2} \\ &\times[R_{zx}^{(e)}A+R_{zy}^{(e)}+R_{zz}^{(e)}B]+\frac{\omega}{\omega_{lh}}[R_{yy}^{(e)}+R_{yz}^{(e)}B] \\ &\left.-Ak_\perp r_{ce}\left(\frac{T_i}{T_e}\right)^{1/2}\frac{u_{de}}{v_{ti}}R_{xy}^{(e)}\right\}d\mathbf{k}.\end{aligned} \tag{117}$$

The above three equations are the sought expressions for our analysis of anomalous transport.[35]

V. SATURATION MECHANISMS

For the numerical analysis of anomalous transport in the MPDT plasma, the last three equations, along with the tensor elements in Eqs. (37)–(44), the linear dispersion relation in Eq. (2) and the transformations in Eqs. (100)–(111) form an *almost* complete set of equations in terms of kr_{ce}, ω/ω_{lh}, γ/ω_{lh} and the seven parameters in Eq. (54). The only lacking equation is one that relates the level of saturated microturbulence $\mathcal{E}_k/n_0T_i$ to those parameters.

The rigorous formulation of this relation is difficult as it concerns the nonlinear saturation mechanism through which the fluctuations, initiated by the instability, reach a steady-state. The saturation mechanism dictates the magnitude and dependencies of the corresponding fluctuating energy density. Since the question of which saturation mechanism is relevant is usually best answered by computer particle simulations and since these simulations have yet to be made for the particular instability studied here, we consider and compare four different saturation mechanisms; ion trapping, electron trapping, ion resonance broadening, and thermodynamic bound. For our purposes here we only quote the resulting expression for each of these saturation models.

A. Thermodynamic limit: The Fowler bound

An upper limit for $\mathcal{E}_t$ was first derived by Fowler[36] (1968) from thermodynamic arguments,

$$(\mathcal{E}_t)_{FB} \leqslant \tfrac{1}{2} n_e m_e u_{de}^2, \tag{118}$$

and simply states that the energy in the turbulent fields cannot exceed the kinetic energy of the electron drift that is fueling the instability. For a convenient incorporation in our particular formulation, we recast the inequality above in terms of the problem's dimensionless parameters and get

$$\frac{(\mathcal{E}_t)_{FB}}{n_0 T_i} \leqslant \frac{m_e}{m_i}\left(\frac{u_{de}}{v_{ti}}\right)^2. \tag{119}$$

B. Saturation by ion trapping

When the excited wave spectrum is narrow due to the dominance of a single wave mode, a monochromatic wave saturation model, such as that behind particle trapping, can prove to be a viable mechanism for saturation. In such a case the saturation dynamics can be governed by the trapping of the particles in the potential wells of the growing mode thus limiting its growth. At saturation one can simply write

$$e\tilde{\phi} = \frac{1}{2} m_i \left(\frac{\omega_r}{k}\right)^2, \tag{120}$$

where ω_r/k is the phase velocity of the dominant mode and we have assumed that the ions are the particles being trapped. Again, we normalize the saturation model for compatibility with transport theory so that, using $e\tilde{\phi} \approx e\tilde{E}/k$ and $\mathcal{E}_k = \epsilon_0 |\tilde{E}_k|^2/2$, the above equation can be rewritten as

$$\frac{(\mathcal{E}_k)_{IT}}{n_0 T_i} = \frac{1}{4(kr_{ce})^2}\left(\frac{\omega_{ce}}{\omega_{pe}}\right)^2 \frac{T_e}{T_i}\left(\frac{\omega_r}{\omega_{lh}}\right)^4. \tag{121}$$

C. Saturation by electron trapping

Electron trapping is probably not a viable saturation mechanism for an instability in which electrons are collisional and are in broad-resonance with the unstable waves. We shall, however, include a model for electron trapping saturation in our calculations for the sake of reference. In analogy with ion trapping, we can write for the electrons as viewed from the ion rest frame

$$e\tilde{\phi} = \frac{1}{2} m_e \left(\frac{\omega_r}{k_z} - u_{de}\right)^2, \tag{122}$$

and after some algebraic manipulations,

$$\frac{(\mathcal{E}_k)_{ET}}{n_0 T_i} = \frac{1}{4(kr_{ce})^2}\left(\frac{\omega_{ce}}{\omega_{pe}}\right)^2 \frac{T_e}{T_i}\left[\Psi \frac{\omega_r}{\omega_{lh}} - kr_{ce}\frac{u_{de}}{v_{te}}\right]^4. \tag{123}$$

D. Saturation by resonance broadening

This mechanism relies on the broadening of wave–particle resonances by the random motion of particles in the turbulent electric field setup by the microinstability.

If resonance broadening is to be important in our case, it would most probably rely on ion dynamics, since the electrons are already broadly resonant with the waves due to collisions and finite-beta effects while the ions are very narrowly-resonant.

Following Gary and Sanderson[37] who applied the Dum–Dupree resonance broadening formula[38] to the ions and found, after taking the velocity average $\int \Delta\omega f_{i_0} d\mathbf{v} / \int f_{i_0} d\mathbf{v}$,

$$(\mathcal{E}_k)_{\mathrm{IRB}} = \frac{1}{2}\epsilon_0 B_0^2 \left(\frac{\omega_r}{k}\right)^2, \tag{124}$$

we specialize the ion resonance broadening model for our dimensionless parameters and obtain

$$\frac{(\mathcal{E}_k)_{\mathrm{IRB}}}{n_0 T_i} = \frac{m_e/m_i}{(kr_{ce})^2}\frac{T_e}{T_i}\left(\frac{\omega_{ce}}{\omega_{pe}}\right)^2 \left(\frac{\omega_r}{\omega_{lh}}\right)^2. \tag{125}$$

VI. CALCULATIONS OF ANOMALOUS TRANSPORT

Armed with the expressions for anomalous transport in Eqs. (115), (116), and (117) along with the tensor elements in Eqs. (37)–(44), the linear dispersion relation in Eq. (2), the transformations in Eqs. (100)–(111) and the saturation models in Eqs. (119), (121), (123), (125), we can now conduct a comparative numerical study of anomalous dissipation.

A. Classical benchmarks

For benchmarks we shall use the following classical expressions for the momentum and energy exchange rates.

For the momentum exchange rate we take the classical Coulomb (electron–ion) collision frequency[19] for momentum relaxation $(\nu_e^p)_{\mathrm{CL}}$

$$(\nu_e^p)_{\mathrm{CL}} = \frac{n_e e^4 \ln\Lambda}{3(2\pi)^{3/2}\epsilon_0 m_e^{1/2} T_e^{3/2}}, \tag{126}$$

where $\Lambda = 9(4/3)\pi n_0 \lambda_{de}^3$ is the plasma parameter. This collision frequency determines the classical Spitzer resistivity

$$(\eta)_{\mathrm{CL}} = \frac{m_e (\nu_e^p)_{\mathrm{CL}}}{n_0 e^2}. \tag{127}$$

For compatibility, we normalize with the lower hybrid frequency and cast the result in terms of our dimensionless parameters, to get

$$\frac{(\nu_e^p)_{\mathrm{CL}}}{\omega_{lh}} = \frac{2}{\sqrt{2\pi}}\left(\frac{m_i}{m_e}\right)^{1/2}\frac{\omega_{pe}}{\omega_{ce}}\frac{\ln\Lambda}{\Lambda}. \tag{128}$$

For a heating rate benchmark we define a classical heating rate, $(\nu_e^T)_{\mathrm{CL}}$, for Joule heating

$$(\nu_e^T)_{\mathrm{CL}} \equiv \frac{1}{n_0 T_e}\frac{\partial}{\partial t} n_e T_e = \frac{2}{3}(\eta)_{\mathrm{CL}} \frac{j^2}{n_0 T_e}, \tag{129}$$

which yields

$$\frac{(\nu^T)_{\mathrm{CL}}}{\omega_{lh}} = \frac{8}{3\sqrt{2\pi}}\left(\frac{u_{de}}{v_{ti}}\right)^2 \frac{T_i}{T_e}\left(\frac{m_e}{m_i}\right)^{1/2}\frac{\omega_{pe}}{\omega_{ce}}\frac{\ln\Lambda}{\Lambda}$$

$$= \frac{4}{3}\left(\frac{u_{de}}{v_{ti}}\right)^2 \frac{T_i}{T_e}\frac{m_e}{m_i}\frac{(\nu_e^p)_{\mathrm{CL}}}{\omega_{lh}}, \tag{130}$$

where the second equation shows the explicit dependence on the collision frequency.

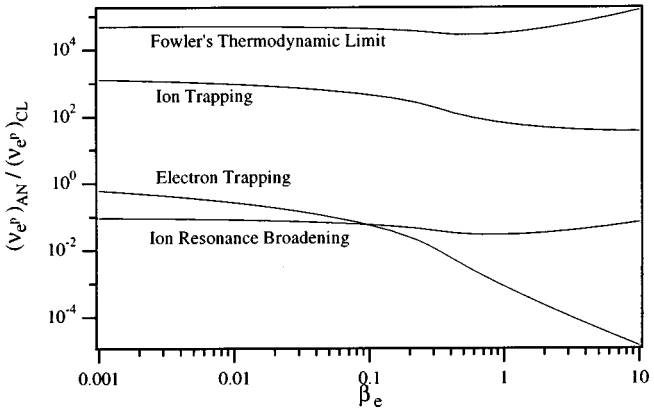

FIG. 4. The anomalous momentum exchange frequency, $(\nu_e^p)_{AN}$, normalized by its classical counterpart and plotted vs the electron beta according to four saturation models. Argon with $u_{de}/v_{ti}=20$, $T_i/T_e=1$, $\nu_e/\omega_{lh}=1$, and $\omega_{pe}/\omega_{ce}=100$.

Finally, we note that in calculating the anomalous rates we approximate the integrals, as commonly done in the literature, by the contribution of the dominant mode only (i.e., for k^{**}), meaning that all the Fourier-decomposed properties are estimated at the doubly maximized growth (i.e., maximized over wavelength and propagation angle).

B. Numerical results

Since β_c and u_{de}/v_{ti} are the two parameters that vary most within the plasma of the MPDT, they were chosen as the varying parameters of the calculations. When β_e is varied, u_{de}/v_{ti} is kept at 20, and when u_{de}/v_{ti} is varied, β_e is set at unity. The other parameters are $m_i/m_e=73{,}300$ (for argon), $T_i/T_e=1$, $\nu_e/\omega_{lh}=1$, and $\omega_{pe}/\omega_{ce}=100$ for continuity with the calculations in Sec. II.

1. Effects of plasma beta

The effects of plasma beta on the resistivity are shown in Fig. 4, where the ratio of anomalous to classical momentum exchange frequency {which is essentially the ratio of the corresponding resistivities [Eqs. (73) and (127)]} is plotted vs beta for the parameters listed above. We note from that plot that with increasing β_e, the curves corresponding to the trapping models significantly deviate from their $\beta_e\rightarrow 0$ asymptotes (which are practically reached at $\beta_e=0.001$). These deviations are due to the electromagnetic corrections to the electrostatic limits, as separated in Eq. (112).

The ion trapping model is of special interest as discussed in Sec. V B especially since it was the only one assumed in the purely electrostatic study of Ref. 14. We see that, when β_e is on the order of unity or greater, as is commonly the case of the MPDT plasma, the anomalous resistivity is an order of magnitude less than that predicted by the purely electrostatic limit.

The reason the anomalous resistivity decreases with increasing beta according to trapping models can be traced to the coupling with the finite polarization modes we discussed in Sec. II E 1. As beta increases, the disturbances to the magnetic field do not have the time to dissipate (low Alfvén velocity) and significant electromagnetic coupling arises. The unstable waves acquire some of the characteristics of the more electromagnetic modes and consequently the most unstable modes shift to lower frequencies. Since the saturation level due to trapping scales with frequency to the fourth power [see Eq. (121)], the end effect is a substantial reduction in the anomalous resistivity.

We note from the plot that the Fowler bound on the calculated rates allows, in principle, for a wide latitude for anomalous resistivity to be important.

We should not expect the electron trapping model to dictate the transport as per arguments already made in previous sections. Furthermore, we should mention that more careful studies of resonance broadening than those made at the time the mechanism was first proposed, have shown that its effects are limited to a redistribution of energy in **k**-space at low plasma beta, and that it does not result in enough dissipation to saturate instabilities such as those being considered here. Therefore, for low β_e, ion trapping seems to be the most viable mechanism.

At these conditions, the anomalous resistivity can be quite dominant (as is observed in Fig. 4), more than two orders of magnitude larger than the classical value, in agreement with the findings of Ref. 14. As β_e increases, saturation by resonance broadening can become more viable especially since the turbulent saturation levels are considerably lower than those for ion trapping (as is clear from the same plot). Whether one or the other mechanism controls saturation depends, at least partly, on whether the spectrum is narrow or broad. Even though experimental data on turbulent fluctuations in the MPDT (Ref. 7) give evidence of a dominant narrow (peaked) spectrum of turbulence in the lower hybrid range, the considerably lower levels of saturation energy implied by the ion resonance broadening mechanism warrant its consideration as a contender in the control of turbulent transport. Of course, this question is perhaps best answered by computer particle simulations.

If ion resonance broadening does take over the control of saturation, anomalous transport can, for the parameters in the above calculations, be brought down below classical levels. One should therefore expect, by virtue of the substantial variability of the plasma beta within the MPD thruster plasma, that there are regions where anomalous resistivity dominates over its classical analog as there are regions where the converse is true.

The same comments we made above also apply for the anomalous electron heating rates that were normalized by the Joule heating rate and plotted in Fig. 5.

It is clear from this plot that when ion trapping dominates, the anomalous heating rate is substantially larger than the electron Joule heating rate. Ion heating rates are not shown here but were found to be similar in both magnitude and dependence to their electron counterparts.

To compare the two rates we have calculated their ratio and plotted the result in Fig. 6.

There is only one curve in this figure because the various saturation models cancel out in the division. Since this ratio is independent of the saturation details, it is more accurate

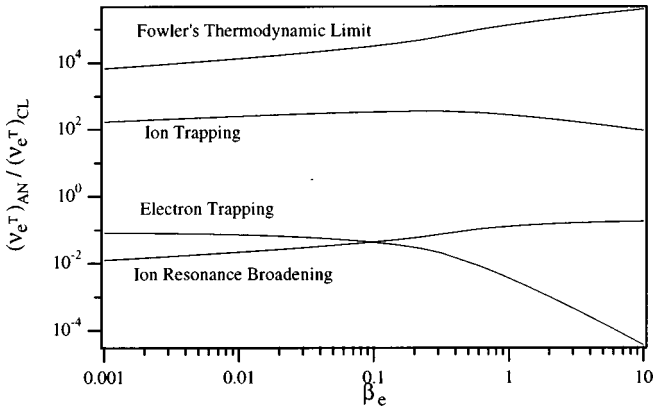

FIG. 5. The anomalous electron heating rate, $(\nu_e^T)_{AN}$, normalized by the Joule heating rate and plotted versus the electron beta according to four saturation models. Argon with $u_{de}/v_{ti}=20$, $T_i/T_e=1$, $\nu_e/\omega_{lh}=1$, and $\omega_{pe}/\omega_{ce}=100$.

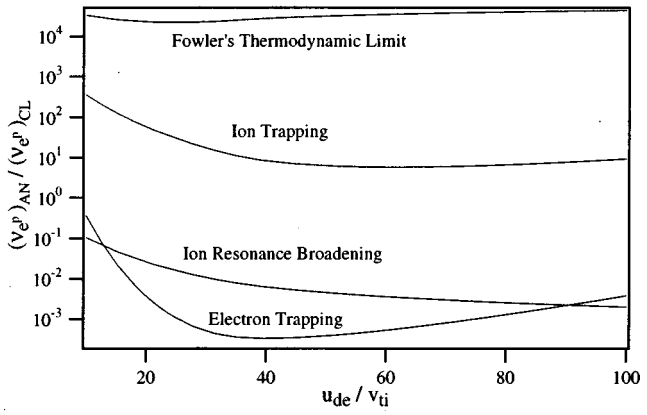

FIG. 7. The anomalous momentum exchange frequency, $(\nu_e^p)_{AN}$, normalized by its classical counterpart and plotted vs the normalized drift velocity according to four saturation models. Argon with $\beta_e=1$, $T_i/T_e=1$, $\nu_e/\omega_{lh}=1$, and $\omega_{pe}/\omega_{ce}=100$.

than the other quantities we have calculated. We note from this figure that, in the electrostatic limit, the two anomalous heating rates are basically equal. This feature is in contrast to the way electrons and ions are heated classically (especially for a heavy atom like argon) and is a well-known characteristic of the (electrostatic) modified two-stream instability as noted in Refs. 15, 16. Since the ions, are heated by the instability-induced turbulence at rates comparable to those of the electrons, and since in the MPDT, the electron energy is strongly tied to excitation and ionization through inelastic collisions, anomalous heating may offer an answer to the long standing question of why the ion temperature in those thrusters is often higher than the electron temperature. Of course, for this argument to be true not only $(\nu_e^T)_{AN}$ must be comparable to $(\nu_i^T)_{AN}$, but the saturation level must be high enough to warrant the dominance of anomalous heating over classical heating. Such is the case when the instability saturates by trapping ions.

The above argument about the relative temperatures is strongest in the electrostatic limit and is in agreement with Ref. 14. When electromagnetic effects start to become important with increasing beta, the same figure shows a degradation of the heating parity towards a progressively preferential heating of electrons. This finding is in agreement with that of Ref. 34, where only the collisionless limit was studied. This degradation in heating parity is not strong enough, however, to weaken the grounds for the above argument concerning the relative temperatures, especially for a heavy atom like argon. Indeed, we see from the same figure that a four-octave increase in beta does not change the order of magnitude of the relative heating ratio.

The increase of preferential electron heating with increasing beta may be partly due to the fact that, at low beta, the instability has its dominant modes oriented at small angles to the magnetic field $[k_z/k \simeq (m_e/m_i)^{1/2}$ or $\Psi \simeq 1]$ and consequently ''perceives'' the electron with an effective mass comparable to that of the ions.[16] As beta increases, electromagnetic coupling with oblique more electromagnetic modes causes the dominant modes to propagate more obliquely, as first noted by Refs. 26 and 39 for the collisionless case. This is also the case when collisions are important as seen from Fig. 2. Consequently, the effective electron mass decreases and the electrons become much easier to heat than the ions.

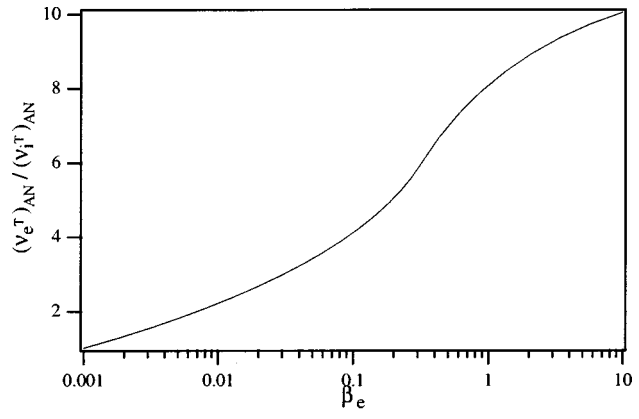

FIG. 6. The anomalous electron heating rate, $(\nu_e^T)_{AN}$, normalized by the anomalous ion heating rate, $(\nu_i^T)_{AN}$, plotted vs the electron beta. Argon with $u_{de}/v_{ti}=20$, $T_i/T_e=1$, $\nu_e/\omega_{lh}=1$, and $\omega_{pe}/\omega_{ce}=100$.

2. Effects of the drift velocity

The effects of the drift velocity are illustrated in the plots of Figs. 7 and 8 for the same parameters as above but with β_e set to unity and u_{de}/v_{ti} varying between 10 and 100.

In reference to Fig. 7 we note that the general decreasing trend of anomalous resistivity with the drift velocity, once the instability is onset is not intuitive (the u_{de}/v_{ti} thresholds for the onset of the instability are not marked on these plots because they are on the order of unity). One would expect that an increase in the free energy source of the instability would enhance the anomalous resistivity effect. In Ref. 14 the same trend was found but no explanation was given.

This trend can be understood once we realize that the scaling of the linear growth rate of the dominant mode

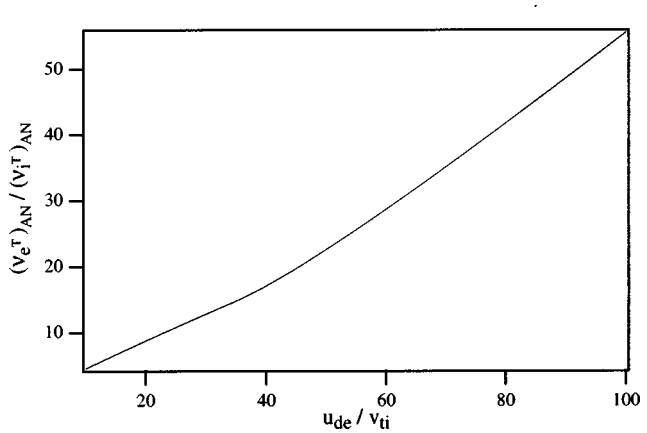

FIG. 8. The anomalous electron heating rate, $(\nu_e^T)_{AN}$, normalized by the anomalous ion heating rate, and plotted for the same conditions as in Fig. 7.

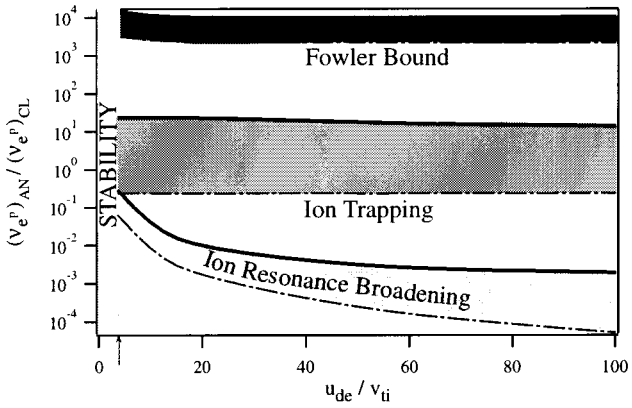

FIG. 9. The anomalous momentum exchange frequency, $(\nu_e^p)_{AN}$, normalized by its classical counterpart and plotted vs the normalized electron drift velocity according to three saturation models. The upper line of each band corresponds to the moderately collisional condition $\nu_e/\omega_{lh}=25$ ($T_e=3$ eV, $n_0=10^{20}\,\mathrm{m}^{-3}$) and the lower (broken) line corresponds to the strongly collisional condition $\nu_e/\omega_{lh}=500$ ($T_e=1.5$ eV, $n_0=1.5\times10^{22}\,\mathrm{m}^{-3}$). Argon with $\beta_e=1$, $T_i/T_e=1$, and $\omega_{pe}/\omega_{ce}=100$.

(which does increase with the drift velocity) does not *necessarily* reflect in weak turbulence (quasilinear) transport scaling since the dependencies of the saturation mechanism (which is extraneous to linear theory) can overwhelm linear trends. This becomes clearer by noting that although an increase in the drift velocity does enhance the linear growth rate of the dominant mode, it also shifts the modes to more oblique propagation and lowers their frequencies.[13] Even though the instability goes to longer wavelength, the dependence of the saturation level for a trapping mechanism [see Eq. (121)] scales with the frequency to the fourth power so that the frequency scaling of the saturation mechanism overpowers the growth scaling of the linear modes. This trend is further accentuated for saturation by electron trapping because, in addition to the above arguments, the saturation level scales with Ψ^4 and Ψ decreases considerably (oblique propagation) with increasing drift velocity. At very high drift, the Doppler shift term in the saturation model [see Eq. (123)] becomes more significant and reverts the trend, which explains the rise of the electron trapping curve in Fig. 7 at high values of u_{de}/v_{ti}.

As expected from the above beta-dependence study, anomalous electron heating rates exceed those of the ions for the present case of $\beta_e=1$. The preferential electron heating is further enhanced by increasing drift velocity as can be seen in Fig. 8. The reason for this behavior is similar to the one given above in the context of electromagnetic enhancement of electron preferential heating. This is so because both increasing beta and increasing drift velocity act to shift the instability toward more oblique propagation thus reducing the large $\bar{m}_e$-effect (where $\bar{m}_e$ is the effective electron mass that scales with the square of ψ) and subjecting the now ''lighter'' electrons to more heating.

C. MPD thruster calculations

We have, in the above calculations, chosen a set of parameters that is generally representative of the MPDT plasma. There is, however, one exception. It is the value of ν_e/ω_{lh} which we have set equal to unity as a compromise between having to represent a collisional plasma and providing a link with previous studies. Moreover, many of the complex interactions between the natural plasma modes, the free energy source and collisions are most pronounced when the collision frequency is on the order of the oscillating frequency. We now, supplement our calculations with results obtained at collisional levels more appropriate of the MPDT plasma.

In order to approximate a typical range for MPDT plasma collisionality, we consider the typical range for the variation of temperature and density. For more detail on how the various parameters of interest vary within the MPDT discharge the reader is referred to the parameter review in Ref. 6. Assuming that T_e varies between 1.5 and 3 eV, while n_0 ranges between 10^{20} and $1.5\times10^{22}\,\mathrm{m}^{-3}$, we can calculate a lower and upper bound for ν_e/ω_{lh} in argon from Eq. (128) to be 25 and 500, respectively, where we have fixed ω_{pe}/ω_{ce} at 100 for compatibility with the above calculations.

For the results shown in Fig. 9 we have chosen to fix beta at unity to preserve electromagnetic effects and varied u_{de}/v_{ti} from 100 down to the threshold of the instability, which, although slightly exaggerated in the figure (vertical hashed region), was at $u_{de}/v_{ti}\simeq1.5$. For each of the three considered mechanisms the plot shows a band whose upper line corresponds to the moderately collisional condition $\nu_e/\omega_{lh}=25$ ($T_e=3$ eV, $n_0=10^{20}\,\mathrm{m}^{-3}$) and whose lower (broken) line corresponds to the strongly collisional condition $\nu_e/\omega_{lh}=500$ ($T_e=1.5$ eV, $n_0=1.5\times10^{22}\,\mathrm{m}^{-3}$).

We note from the figure that, although the Fowler bound allows for a large microturbulent contribution to the resistivity, ion resonance broadening might cause the instability to saturate at low levels. Even though arguments have been advanced recently discounting the importance of such a mechanism, it should not be totally discounted pending strong evidence from computer particle simulations and/or dedicated experiments.

We furthermore see that, in the case of ion trapping saturation, once the instability is onset, the importance of anomalous resistivity in the MPDT plasma is not as much dictated

by the drift velocity (since the two limiting curves are quite flat), as one would intuitively suspect, as it is dictated by the level of collisionality. Indeed, if collisionality is strong, anomalous resistivity can be kept below classical levels even if the instability is excited and even if ion trapping is responsible for saturation, as is clear from the plot. It must be said, however, that even in the case of high collisionality ($\nu_e/\omega_{lh} \simeq 500$) where anomalous resistivity is kept below classical levels, it is still a finite fraction of its classical counterpart (about 25% in the above calculations), as can be seen from the same plot (again, assuming ion trapping saturation). This implies that low density regions of the MPDT discharge, such as regions depleted from charge due to the $j_z B_\theta$ Lorentz force component, tend to be more vulnerable to anomalous resistivity than denser (or more collisionally dominated) regions. This trend is in agreement with the well-known fact that dissipation in charged-depleted regions of the device, like the anode vicinity,[40] is enhanced by weak collisionality.

Stated differently, under MPDT plasma conditions and for the microinstabilities in question, the level of anomalous contribution to resistivity is dictated to a large extent by the parameter ν_e/ω_{lh}. It is interesting to note that this parameter is directly related to the electron Hall parameter Ω_{H_e}. Indeed, it is just the inverse of the electron Hall parameter scaled by the square root of the mass ratio

$$\Omega_{H_e} \equiv \frac{\omega_{ce}}{\nu_e} = \frac{(m_i/m_e)^{1/2}}{\nu_e/\omega_{lh}}. \tag{131}$$

The known scaling of the anode voltage drop with the Hall parameter (see for instance the measurements in Ref. 40) that constitutes one of the most dissipative sinks for the low-power MPDT is thus another invariant behavioral trait of the accelerator that could possibly be explained by the effects of microinstabilities.

The anomalous ion and electron heating rates were also calculated and found to have the same general trends as those of the anomalous resistivity.

VII. ANOMALOUS TRANSPORT MODELS FOR INCLUSION IN FLUID CODES

We now seek anomalous transport expressions that would be suitable for inclusion in fluid codes for the numerical simulation of MPDT flows. This may be accomplished by carrying *a priori* calculations of the relevant anomalous transport for the expected parameter-space covered by typical numerical simulations then fitting the calculations with polynomial expressions.

In general the description of microstability (and hence microturbulence in our model) depends on the following set of eight independent macroscopic parameters:

$$kr_{ce},\ \Psi,\ \frac{m_i}{m_e},\ \frac{\omega_{pe}}{\omega_{ce}},\ \beta_e,\ \frac{u_{de}}{v_{ti}},\ \frac{T_i}{T_e},\ \Omega_{H_e}. \tag{132}$$

The first two parameters are varied to growth-maximize the solutions. Since all anomalous transport rates used here were calculated at maximum growth these two parameters drop out of the final models. The mass ratio m_i/m_e is that of argon. All solutions were found to be very insensitive to the fourth parameter, namely ω_{pe}/ω_{ce}, as long as that ratio exceeded 10 which was the case for the simulations conducted so far.[10,11] Similarly, the solutions were weakly dependent on β_e as long as the electron Hall parameter, Ω_{H_e} did not exceed 10.

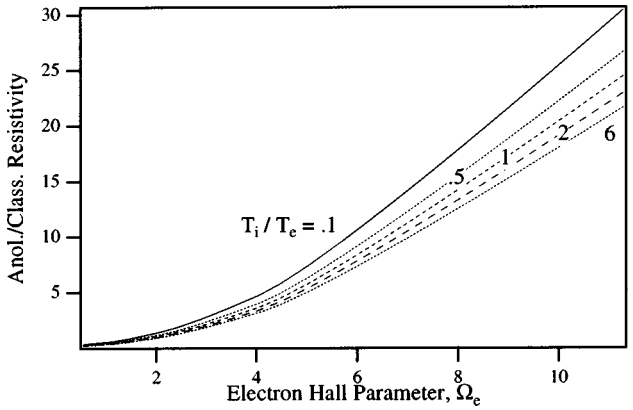

FIG. 10. Ratio of anomalous resistivity to classical resistivity for argon as a function of the electron Hall parameter and T_i/T_e with u_{de}/v_{ti} exceeding 1.5.

The last three parameters are the most important for our problem. First, u_{de}/v_{ti} must reach a threshold for the instability to be excited and hence for anomalous transport to be operative. For the entire region of the investigated parameter-space that threshold was very near 1.5. Second, the ion to electron temperature ratio plays a role in scaling the level of turbulence. Invariably for our parameter-space, it was found that increasing T_i/T_e causes a devaluation of anomalous transport. The most important of all the macroscopic parameters turned out to be the last one namely the electron Hall parameter Ω_{H_e}.

The anomalous resistivity η_{AN}

$$\eta_{AN} \equiv \frac{m_e(\nu_e)_{AN}}{e^2 n_e}, \tag{133}$$

calculated using the theory presented in the above sections, and normalized by its classic counterpart $\eta_{\mathrm{CL}} \equiv m_e \nu_e / e^2 n_e$ is shown in Fig. 10. It is important to note that an increase in the electron Hall parameter for typical values of T_i/T_e leads to a very significant increase in the anomalous resistivity *if* the parameter u_{de}/v_{ti} is above the stability threshold. It is interesting to note that the scaling of this ratio with the Hall parameter is in general agreement with that inferred by Gallimore *et al.*[40] from measurements in the anode region and the more direct and recent measurements of Black *et al.*[12]

A similar plot is shown in Fig. 11 for the ion heating rate $(\nu_i^T)_{AN}$ normalized by the Coulomb frequency.

A two-parameter, variable cross-term, least square fit was made to the calculated rates shown in Figs. 10 and 11 in order to make them suitable for inclusion in plasma fluid flow codes.

The resulting two-parameter interpolating polynomial for $(\nu_i^T)_{AN}/\nu_{ei}$ has an average accuracy of 15% and reads[41]

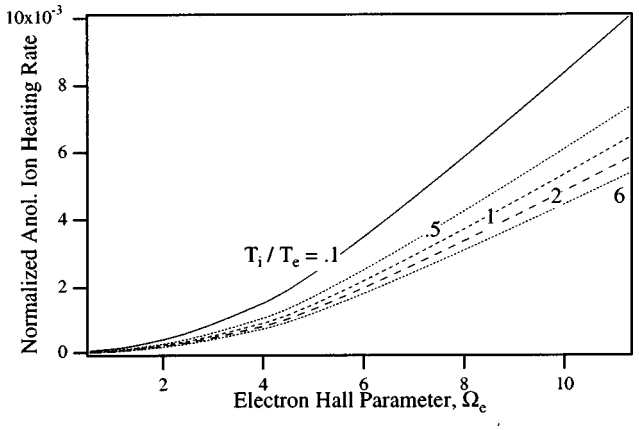

FIG. 11. Anomalous ion heating rate for argon normalized by the Coulomb frequency as a function of the electron Hall and T_i/T_e with u_{de}/v_{ti} exceeding 1.5.

$$\frac{(\nu_i^T)_{AN}}{\nu_{ei}} = 5.36\times10^{-5} + 1.29\times10^{-5}\Omega_{He} + 6.03\times10^{-6}\Omega_{He}^2 + 9.44\times10^{-8}\Omega_{He}^3 + \frac{T_i}{T_e}(-7.55\times10^{-7} - 5.41\times10^{-6}\Omega_{He} - 3.93\times10^{-6}\Omega_{He}^2). \quad (134)$$

The ions are heated by the turbulent fluctuations at a rate $(Q_i)_{AN} = \frac{3}{2}(\nu_i^T)_{AN} T_h$.

The effective conductivity introducing the anomalous resistivity effect to a flow simulation code is

$$\sigma_{\text{eff}} = \frac{e^2 n_e}{m_e(\nu_{ei} + (\nu_e^P)_{AN})}, \quad (135)$$

where $(\nu_e^P)_{AN}$ is the electron-wave momentum exchange frequency, which is again computed through an interpolating polynomial of average accuracy of 10%,

$$\frac{(\nu_e^P)_{AN}}{\nu_{ei}} = 0.192 + 3.33\times10^{-2}\Omega_{He} + 0.212\Omega_{He}^2 - 8.27\times10^{-5}\Omega_{He}^3 + \frac{T_i}{T_e}(1.23\times10^{-3} - 1.58\times10^{-2}\Omega_{He} - 7.89\times10^{-3}\Omega_{He}^2). \quad (136)$$

The use of these models in a plasma fluid flow code may proceed in the following way. At all the gridpoints in the simulation domain where $u_{de}/v_{ti} < 1.5$ both, $(\nu_e^P)_{AN}$ and $(\nu_i^T)_{AN}$ are set to zero and all transport is assumed purely classical. Otherwise, the anomalous rates are computed from the above polynomials using the instantaneous macroscopic parameters and folded back into the flow equations at every time step thus insuring self-consistency. This was done in Refs. 10 and 11.

VIII. CONCLUSIONS

The dielectric tensor for a magnetoactive, current-carrying, collisional and finite-beta plasma was derived using kinetic theory without making the electrostatic assumption.

A parametric study of the resulting linear dispersion relation for plasma parameters typical of the MPDT showed that a mixed polarization mode can be easily driven unstable by the cross-field current. Collisions and finite-beta effects were found to change the character of the instability from previous collisionless and/or electrostatic treatments.

Using the linear description and plasma weak turbulence theory, a second-order model of wave–particle transport and anomalous dissipation was developed. Assuming ion trapping to be the saturation mechanism, our calculations show that the saturation of the collisional generalized lower hybrid drift instability (GLHDI), which has been observed in the MPDT plasma,[7,8] can cause a severe enhancement to the local resistivity and the bulk heating rate of both ions and electrons. It can also cause a preferential effective heating of the ions and enhance both heating and resistivity in regions of low collisionality (high electron Hall parameters).

Polynomial expressions of the relevant transport coefficients cast solely in terms of macroscopic parameters were also obtained for inclusion in plasma fluid codes. The anomalous resistivity was shown to be most sensitive to the electron Hall parameter. This theoretically predicted scaling was recently confirmed by independent experimental measurements.[12]

ACKNOWLEDGMENTS

This work was supported by grants from the U.S. Air Force Office of Scientific Research and the National Aeronautics and Space Administration-Jet-Propulsion Laboratory.

[1] V. M. Nerheim and A. J. Kelly, NASA-JPL Technical Report No. 32-1196, NASA-JPL, Pasadena, CA, USA 1968 (National Aeronautics and Space Administration, Washington, D.C.).
[2] J. S. Sovey and M. A. Mantenieks, American Institute of Aeronautics and Astronautics, Washington, D.C., 1992, AIAA-88-3211.
[3] R. M. Myers, M. A. Mantenieks and M. R. LaPointe, American Institute of Aeronautics and Astronautics, Washington, D.C., 1992, AIAA-91-3568.
[4] E. Y. Choueiri, J. Propul. Power **14**, 744 (1998).
[5] A. C. Ducati, G. M. Giannini, and E. Muehlberger, AIAA J. **2**, 1452 (1964).
[6] D. L. Tilley, Master's thesis, Princeton University, Princeton, NJ, 1991.
[7] D. L. Tilley, E. Y. Choueiri, A. J. Kelly, and R. G. Jahn, J. Propul. Power **12**, 381 (1996).
[8] E. Y. Choueiri, A. J. Kelly, and R. G. Jahn, in *Proceedings of the 22nd International Electric Propulsion Conference* (CentroSpazio, Viareggio, Italy, 1991), IEPC-91-100. Copies can be ordered from CentroSpazio, Via A. Ghirerdesca, 5, 26014 Ospedallto, Pisa, Italy.
[9] E. Y. Choueiri, A. J. Kelly, and R. G. Jahn, American Institute of Aeronautics and Astronautics, Washington, D.C., 1992, AIAA-92-3739.
[10] G. Caldo, E. Y. Choueiri, A. J. Kelly, and R. G. Jahn, American Institute of Aeronautics and Astronautics, Washington, D.C., 1992, AIAA-92-3738.
[11] G. Caldo, E. Y. Choueiri, A. J. Kelly, and R. G. Jahn, in *Proceedings of the 23rd International Electric Propulsion Conference* (PRIMEX Aerospace, Seattle, WA, 1993), IEPC-93-072. Copies can be ordered from Ms. Joyce Armstrong, Primex Aerospace, P.O. Box 97009, Redmond, WA 98073-9709.
[12] D. C. Black, R. M. Mayo, and R. W. Caress, Phys. Plasmas **4**, 3581 (1997).
[13] E. Y. Choueiri, A. J. Kelly, and R. G. Jahn, American Institute of Aeronautics and Astronautics, Washington, D.C., 1990, AIAA-90-2610.
[14] D. Hastings and E. Niewood, J. Propul. Power **9**, 361 (1991).
[15] J. B. McBride and E. Ott, Phys. Lett. **39A**, 363 (1972).
[16] J. B. McBride, E. Ott, J. P. Boris, and J. H. Orens, Phys. Fluids **15**, 2367 (1972).

[17]A. I. Paytak and V. L. Sizonenko, Sov. Phys. Tech. Phys. **19**, 635 (1974).
[18]J. B. Hsia, S. M. Chiu, M. F. Hsia, R. L. Chou, and C. S. Wu, Phys. Fluids **22**, 1737 (1979).
[19]D. G. Swanson, *Plasma Waves* (Academic, San Diego, 1989).
[20]P. L. Bhatnagar, E. P. Gross, and M. Krook, Phys. Rev. **94**, 511 (1954).
[21]J. D. Callen and G. E. Guest, Nucl. Fusion **13**, 87 (1973).
[22]C. L. Chang, H. K. Wong, and C. S. Wu, Phys. Rev. Lett. **65**, 1104 (1990).
[23]E. Y. Choueiri, Ph.D. thesis, Princeton University, Princeton, NJ, 1991.
[24]We have found that, for the range of parameters covered in our investigations, cyclotron summations with the seven terms, $n=0,\pm1,\pm2,\pm3$ are required to reduce the error below 2%.
[25]D. S. Lemons, Ph.D. thesis, College of William and Mary, Williamsburg, VA, 1977.
[26]C. S. Wu, Y. M. Zhou, S. T. Tsai, and S. C. Guo, Phys. Fluids **26**, 1259 (1983).
[27]A. A. Vedenov, E. P. Velikhov, and R. Z. Sagdeev, Nucl. Fusion **1**, 82 (1961).
[28]W. E. Drummond and M. N. Rosenbluth, Phys. Fluids **5**, 1507 (1962).
[29]A. A. Galeev and R. Z. Sagdeev, in *Basic Plasma Physics II*, edited by A. Galeev and R. Sudan (North–Holland, Amsterdam, 1984), Part 4.
[30]R. C. Davidson and N. A. Krall, Nucl. Fusion **17**, 1313 (1977).
[31]K. Papadopoulos, in *Collisionless Shocks in the Heliosphere: A Tutorial Review*, edited by R. Stone and B. Tsurutani (American Geophysical Union, Washington, D.C., 1985).
[32]R. C. Davidson, *Methods in Nonlinear Plasma Theory* (Academic, New York, 1972).
[33]E. M. Lifshitz and L. P. Pitaevskii, *Statistical Physics*, 3rd ed. (Pergamon, Oxford, 1980), Part 1.
[34]D. Winske, M. Tanaka, C. S. Wu, and K. B. Quest, J. Geophys. Res. **90**, 123 (1985).
[35]The authors of Ref. 34 have derived expressions for the anomalous heating rates of ions and electrons in finite-beta plasmas. Their expressions differ from ours because of a difference in evaluating the ensemble-averages. In going from Eq. (91) to Eq. (92) above, for instance, these authors would neglect in the summation the cross-terms $\tilde{E}_l\tilde{E}_m$ with $l\neq m$ [see Eqs. (14) and (15) of that paper]. There does not seem to be, however, a valid *a priori* reason to neglect such cross-terms. Indeed, had we dropped these terms, the last term of the sum in the integrand of Eq. (99) would vanish. This term, $2R_{zz}^{(e)}B^2$, was found to be important for many situations we have investigated numerically. Furthermore, had we dropped the cross-terms it would not have been possible to recover the electrostatic contribution from Eq. (112) in the $\beta\rightarrow0$ limit.
[36]T. K. Fowler, in *Advances in Plasma Physics*, edited by A. Simon and W. Thompson (Interscience, New York, 1968), pp. 201–226.
[37]S. P. Gary and J. J. Sanderson, Phys. Fluids **24**, 638 (1981).
[38]C. T. Dum and T. H. Dupree, Phys. Fluids **13**, 2064 (1970).
[39]S. T. Tsai, M. Tanaka, I. D. Goffey Jr., E. H. Da Jornada, and C. S. Wu, J. Plasma Phys. **32**, 159 (1984).
[40]A. D. Gallimore, A. J. Kelly, and R. G. Jahn, J. Propul. Power **9**, 361 (1993).
[41]Due to a typographical error in the polynomial corresponding to Eq. (134) appearing in Ref. 9, the third term in the polynomial appearing in that paper must be multiplied by 10.